The Fluctuating Cell-Specific Light Environment and Its Effects on Cyanobacterial Physiology[1][OPEN]

Björn Andersson,[a] Chen Shen,[b] Michael Cantrell,[a] David S. Dandy,[b] and Graham Peers[a,2,3]

[a]Department of Biology, Colorado State University, Fort Collins, Colorado 80523
[b]Department of Chemical and Biological Engineering, Colorado State University, Fort Collins, Colorado 80523

ORCID IDs: 0000-0003-4297-2927 (B.A.); 0000-0003-3829-6233 (M.C.); 0000-0003-3254-0717 (D.S.D.); 0000-0002-3590-7820 (G.P.).

Individual cells of cyanobacteria or algae are supplied with light in a highly irregular fashion when grown in industrial-scale photobioreactors (PBRs). These conditions coincide with significant reductions in growth rate compared to the static light environments commonly used in laboratory experiments. We grew a dense culture of the model cyanobacterium *Synechocystis* sp. PCC 6803 under a sinusoidal light regime in a bench-top PBR (the Phenometrics environmental PBR [ePBR]). We developed a computational fluid dynamics model of the ePBR, which predicted that individual cells experienced rapid fluctuations (~6 s) between 2,000 and <1 μmol photons m^{-2} s^{-1}, caused by vertical mixing and self-shading. The daily average light exposure of a single cell was 180 μmol photons m^{-2} s^{-1}. Physiological measurements across the day showed no in situ occurrence of nonphotochemical quenching, and there was no significant photoinhibition. An ex situ experiment showed that up to 50% of electrons derived from PSII were diverted to alternative electron transport in a rapidly changing light environment modeled after the ePBR. Collectively, our results suggest that modification of nonphotochemical quenching may not increase cyanobacterial productivity in PBRs with rapidly changing light. Instead, tuning the rate of alternative electron transport and increasing the processing rates of electrons downstream of PSI are potential avenues to enhance productivity. The approach presented here could be used as a template to investigate the photophysiology of any aquatic photoautotroph in a natural or industrially relevant mixing regime.

Targeted improvement of photosynthetic efficiency has been suggested to form the basis for the next generation of improved biofuel and crop strains (Zhu et al., 2010; Ort et al., 2015). Specific targets have included reducing energy losses associated with the photoprotective response of photosynthesis, which are engaged in plants grown in the field. For instance, tuning the capacity for light energy dissipation has resulted in an increase in biomass production of tobacco (*Nicotiana tabacum*) by 30% in field trials (Kromdijk et al., 2016). Translating this approach to aquatic, photoautotrophic microbes such as cyanobacteria requires a better understanding of the photophysiology of growth in mass culture to choose appropriate engineering targets (Simionato et al., 2013; Peers, 2014).

Physiologists are gaining an appreciation of how light behaves in the complex three-dimensional canopy of plants while also measuring how this variable light impacts photosynthetic processes. Several recent studies have used digital renderings of plant morphology along with changes in incident solar irradiation and angle to demonstrate that leaves in the lower canopy are exposed to rapid fluctuations in light fluxes (Retkute et al., 2018). Furthermore, modeling of leaf physiology suggests that lower leaves are unable to efficiently utilize short increases in light flux (Townsend et al., 2018). Additionally, plants grown in fluctuating light versus square-wave light have a decrease in overall carbon assimilation, presumably due to negative feedback on photosynthesis (Vialet-Chabrand et al., 2017). There are several mechanisms that can lead to this decrease in photosynthetic efficiency, including nonphotochemical quenching (NPQ), changes in enzyme activation states, and limiting CO_2 diffusion into the chloroplast (Kaiser et al., 2018).

[1]This work was supported by the National Science Foundation (grant no. NSF EFRI–1332404). Methods used in this manuscript were developed with the support of the United States Department of Energy, Office of Science, Biological and Research Division (contract no. DE–SC0008595). Additional financial support was provided through grants from the Fulbright Program, the American–Scandinavian Foundation, and the Sixten Gemzeus Foundation. The funding sources had no involvement in the study design, analysis of the data, journal of submission, or other decisions regarding the manuscript.

[2]Author for contact: graham.peers@colostate.edu.
[3]Senior author.

The author responsible for distribution of materials integral to the findings presented in this article in accordance with the policy described in the Instructions for Authors (www.plantphysiol.org) is: Graham Peers (graham.peers@colostate.edu).

G.P. and D.S.D. developed the project concept and designed the overall study; B.A. carried out the physical experiments with *Synechocystis*, designed individual sampling strategies, and analyzed physiological data; C.S. developed the computational fluid dynamic model and carried out in silico analysis of these data; M.C. developed the membrane inlet mass spectrometry setup and carried out these experiments and analyses; B.A. and G.P. drafted the article; all authors critically reviewed and contributed text to the final version of the article.

[OPEN]Articles can be viewed without a subscription.
www.plantphysiol.org/cgi/doi/10.1104/pp.19.00480

Microbial autotrophs have evolved under light regimes that bear little resemblance to those of mass cultivation, where light is supplied in a highly irregular fashion. In photobioreactors (PBRs), light fluctuates on a seasonal and diurnal basis, but also at a much faster time scale due to the high density of the culture, which causes self-shading (Posten, 2009). From the perspective of a single photosynthetic cell, the latter translates into rapid fluctuations between full sunlight and darkness throughout the day. Little is known about how this light environment affects the photophysiology of microbial autotrophs due to our limited understanding of the pattern of light fluctuations in PBRs. This is compounded by the difficulties of studying photosynthesis in situ in these large-scale reactors.

In addition to the rapid fluctuations in light caused by self-shading, outdoor PBRs experience a gradual increase/decrease in light intensities at dawn and dusk. At noon, light intensities peak at irradiances that are higher than the light-harvesting capacity. This can lead to an increased rate of reactive oxygen species formation and subsequent oxidative damage to the cells (Erickson et al., 2015). Microbial oxygenic phototrophs have evolved several photoprotective mechanisms to dissipate this excess light energy, including NPQ and modification to linear electron flow (see review by Derks et al. [2015] and Jallet et al. [2016b]). These mechanisms reduce the probability for reactive oxygen species formation.

The orange carotenoid protein (OCP) is responsible for photo-protective NPQ in phycobilisome-containing cyanobacteria. OCP-related NPQ is induced proportionally to the intensity of blue light and not in response to acidification of the lumen (Wilson et al., 2006). State transition is another NPQ mechanism that cyanobacteria use to redistribute light energy between the two photosystems through physical movement of the phycobilisome. Cyanobacteria also use state transitions to optimize photon utilization under low light (Emlyn-Jones et al., 1999). The process is regulated by the redox state of the plastoquinone pool and is very rapid, occurring within seconds of changes in light conditions (Mullineaux and Allen, 1990; Mullineaux and Emlyn-Jones, 2005).

Cyanobacteria also have a complicated electron transport chain downstream of PSII. Electrons can be diverted from linear electron transport to reduce oxygen at various points, which is used as photoprotection or to modify the ATP:NADPH production ratio (Ermakova et al., 2016). The mechanisms include two respiratory terminal oxidases, and flavodiiron (flv) proteins. Flv protein can operate either to maintain function of PSII (Bersanini et al., 2014, 2017) or to divert electrons downstream of PSI (Allahverdiyeva et al., 2013). Despite a growing understanding of the molecular complexity of cyanobacterial photoprotection under various laboratory light regimes, very little is known about how these mechanisms operate under complex natural or industrially relevant light conditions.

Computational fluid dynamics (CFD) offers a highly accurate and precise method for tracking the movement of gases and liquids in turbulent environments (Jameson, 1995). CFD has been used to optimize heterotrophic bioreactors by predicting nutrient mixing and gas exchanges (Dhanasekharan et al., 2005; Hutmacher and Singh, 2008; Devarapalli et al., 2009). CFD studies have also predicted scalability and velocity fields of algal raceway ponds (Liffman et al., 2013; Prussi et al., 2014) and the light environment of closed tubular and airlift PBRs (Barbosa et al., 2003; Huang et al., 2015). These studies predict that light/dark (L/D) oscillations are highly variable in closed PBRs, ranging between 10 and 0.01 s^{-1}, depending on reactor design.

A limited set of studies have investigated the effect of rapid L/D fluctuations on photosynthesis and suggest that 1,000–0.1 s^{-1} oscillations may actually benefit productivity through recycling of rate-limiting metabolites in the Calvin-Benson-Bassham cycle (Takache et al., 2015) and reduced photodamage (Nedbal et al., 1996). However, these considerations tend to be based on square-wave oscillations and do not take into consideration changes in incident light associated with natural daylight. CFD offers a refined method to predict light and mixing environments in physical reactors. These data can then be used to investigate the effects of complicated light regimes on photosynthesis and other cellular functions.

Understanding the complex interactions between dynamic light and photophysiology is crucial to metabolic engineering of cyanobacteria and algae. Cyanobacteria are excellent candidates for metabolic engineering for enhanced production of biofuels and other economically relevant compounds due to their relatively simple structure, metabolic network, small genome, and amenability to genetic modification (Kaneko et al., 1996; Koksharova and Wolk, 2002; Angermayr et al., 2015). This study aimed to answer three questions: (1) how does the light environment of a PBR change on a diurnal basis from the perspective of a single cell, (2) how do these light changes affect photosynthesis and culture productivity, and (3) which photoprotective mechanisms are active in situ? To this end, we grew the model cyanobacterium *Synechocystis* sp. strain PCC 6803 at an industrially relevant density in one of the most commonly used bench-scale PBRs: the Phenometrics environmental PBR (ePBR). We used CFD to model the cell-specific light environment of the ePBR and monitored rates of cell division and carbon accumulation. Finally, we measured photosynthetic capacity across the day and subjected cultures to the predicted light model ex situ to investigate the photophysiological responses to the rapidly changing light environment.

RESULTS

Growth in the ePBR

We conducted experiments on batch cultures of *Synechocystis* sp. PCC 6803 in the ePBRs to establish growth traits. The culture grew at an initial exponential

rate of 12.5 ± 1.0 h (n = 6), but as it became denser, and the light penetration was reduced, it entered the linear growth phase at around 0.5×10^8 cells mL^{-1} (Fig. 1A). The culture grew linearly from that point onward until it entered the stationary phase at 8×10^8 cells mL^{-1}, most likely due to inorganic nutrient depletion (Supplemental Fig. S1A).

Based on the batch growth observation, we set the experimental density of the semicontinuously grown ePBR cultures at midlinear growth and maintained it at $1.4 \times 10^8 \pm 0.1 \times 10^8$ cells mL^{-1} (n = 90, ±SD) during the experimental sampling (days 6–7). This corresponded to an optical density at 750 nm (OD_{750}) of 0.73. To avoid CO_2 limitation, the pH of the ePBR cultures was maintained at 7.5 ± 0.1 (n = 58) throughout the experiments by continuous sparging with 1% CO_2-enriched air, and the harvesting density was four times lower than that observed in the stationary phase. This suggests that the ePBR culture was growing linearly due to light limitation. The doubling time at this specific density was 75 ± 22 h. The doubling time did not change between days 6 and 7 (Fig. 1B), suggesting tha the culture had acclimatized to the experimental conditions.

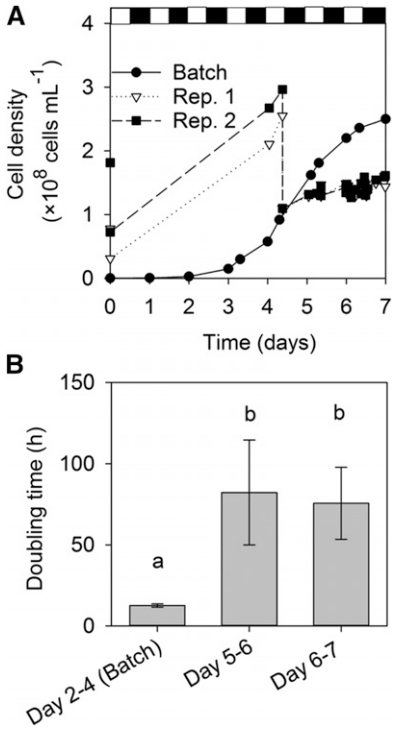

Figure 1. Growth curves, experimental densities, and growth rates. A, Examples of batch culture grown in the ePBR under sinusoidal light (Batch) and during the semicontinuous cultivation experiment (Rep. 1 and 2). Note that the cell densities drop at specific sampling points due to dilution with fresh media. B, Comparison of doubling times during low-density exponential growth (Batch.) and the first day of semicontinuous growth (days 5–6) and the sampling day (days 6–7). Differences in growth rates were analyzed using one-way ANOVA, $F_{2,15} = 17.311$, $P < 0.001$. Error bars = SD (n = 6, letters indicate statisticaly signifance differences).

CFD-Mediated Description of Mixing

We aimed to understand the scale of temporal changes in the light environment from the perspective of a single cell, which was predicted to change rapidly due to intense mixing and self-shading. To this end, we used CFD coupled with in situ measurements of the light intensity in the ePBR to generate a high-resolution model of the cell-specific light environment over the course of one day. A schematic of the ePBR is shown in Supplemental Figure S2.

The movement of a single particle, hereafter referred to as a cell, was highly stochastic on the second timescale, but over the course of several minutes, a repetitive pattern emerged as a cell moved throughout the water column by the action of the stir bar and gas sparging. These forces caused the cells to spiral upward along the wall of the vessel and sink down the middle (Fig. 2). To further understand the driving forces that moved the suspended cells, we looked at the velocity contours and vectors of four horizontal cross sections and one vertical cross section (Fig. 3). The results show that there were strong rotational motions in the horizontal plane due to the activity of the stir bar (Fig. 3B), which was spinning at 500 rpm. A high-velocity region (up to 0.3 m s^{-1}) was observed at 9-, 14-, 19-, and 23-cm depths, as shown in the cross sections of Figures 3, A and D, caused by rising gas bubbles. The velocity magnitude was higher near the outer boundary of the vessel than at the center since the angular velocity is similar in each cross section. The velocity of fluid movement near the boundary also increased near the stir bar at the bottom (Fig. 3C), and the mean velocities of cross sections from top to bottom were 0.12, 0.16, 0.18, and 0.20 m s^{-1}, respectively. The overall mean velocity in the ePBR was 0.15 m s^{-1}. These results suggest that the fluid rotated with a higher angular velocity at the bottom than at the surface, which is reasonable because the angular momentum is transferred by the stir bar at the bottom and dissipates as the fluid moves upward. The vessel is also slightly cone shaped, which means that more volume exists near the surface than the bottom of the vessel, further decreasing the rotational energy.

The velocity profile in the vertical cross section showed that the fluid has a stronger convection motion in the vertical direction (Fig. 3D), causing the particles to approach the surface along the sides and sink down near the center. The CFD model also showed that the rising bubble column caused occasional disturbances when particles were rapidly lifted toward the surface, or shifted to a downward convection before reaching the surface.

We corroborated the in silico CFD modeling results with high-speed camera recordings of neutrally buoyant beads (1-mm diameter, according to the methods used by Prussi et al. [2014]; please see Supplemental Data Set S1 for more detail). A video showed that the bubble column and rotational momentum predicted by the CFD model cells could be seen in situ as well

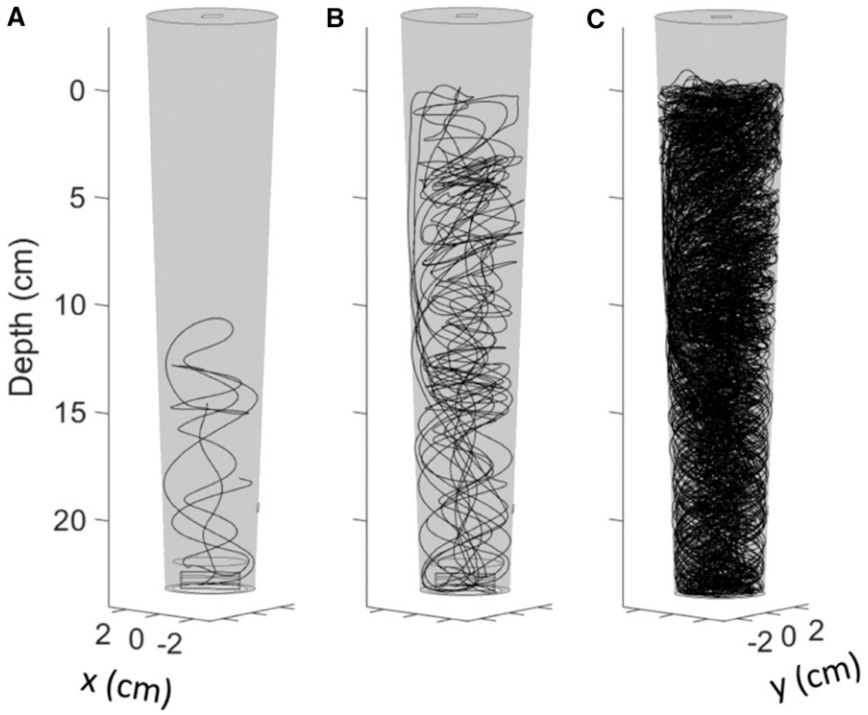

Figure 2. *In silico* tracking of a particle (single cells) in the ePBR using CFD. Tracking of the position of a single particle (cell) is shown for different periods of time: 6 s (A), 60 (B), and 600 s (C).

(Supplemental Fig. S3; Supplemental Video). Special attention was given to the CFD model of the gas inlet. Surface tension caused the gas phase to collect in the ePBR near the inlet. Once the gas volume became large enough, a bubble was formed and then left the inlet and navigated the liquid phase before finally entering the headspace of the vessel. Although the shape of the inlet and the merging behavior of the bubbles near the inlet were simplified in the CFD model, the shapes and behaviors of the bubbles and the gas–liquid interface are captured accurately (Supplemental Video). The location where the bubbles reach the interface of the ePBR wall

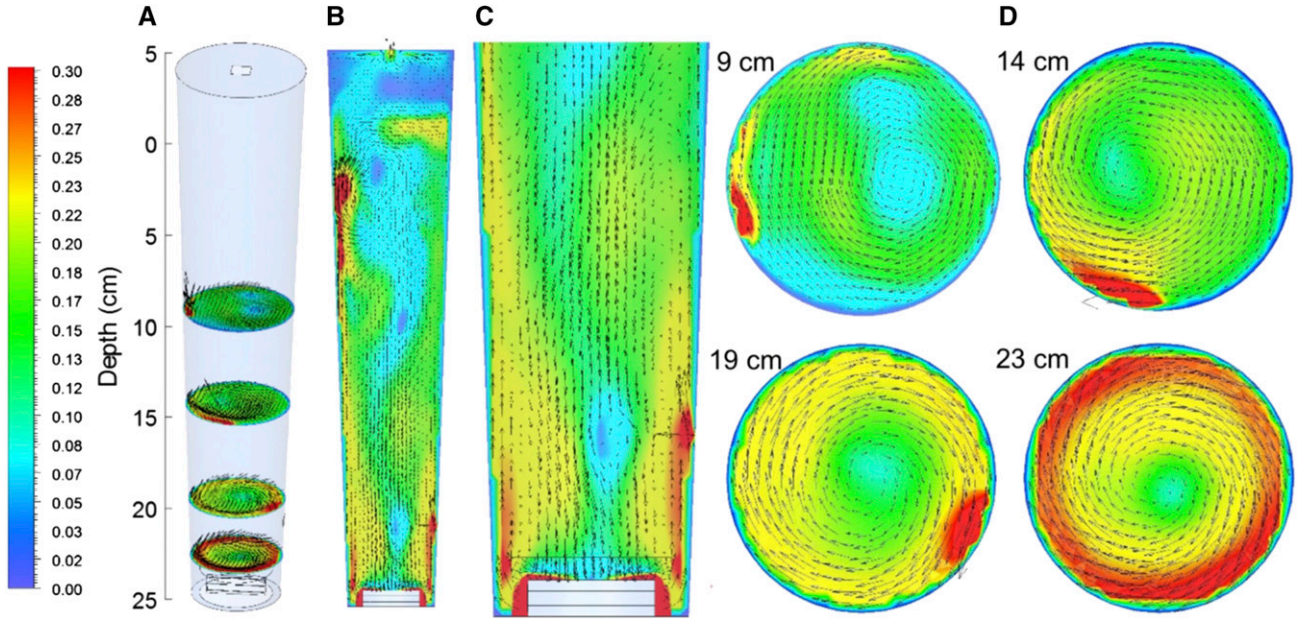

Figure 3. A snapshot of the CFD model showing instantaneous velocity vectors and contours in the ePBR vessel. A, Four different horizontal cross sections illustrated in the ePBR. B, Vertical cross section. C, Close-up of lower half of the ePBR with stir bar in white and red zone to the right coinciding with the entry point of the bubble stream. D, Vertical overviews or the transects shown in A. Color indicates the velocity of the fluid in m s^{-1}, and arrows indicate direction and magnitude.

was also comparable to the simulated result, suggesting that the bubble column was accurately modeled.

The Cell-Specific Light Environment

The vertical light environment of the ePBR changed dramatically. Only 1% of the surface light remained at half the maximum depth of the vessel (Fig. 4A). We translated the movement of a cell with respect to culture depth to the light intensity experienced over time. Most commonly, cells could be mixed from the surface to the bottom of the vessel, or vice versa, within a range of 0.8–6.4 s (Supplemental Fig. S4). This movement resulted in very rapid changes in the cell-specific light exposure due to the exponential extinction of light (Fig. 4C). Cells oscillated between near darkness (>10-cm depth; <1.5% of surface PAR), in the bottom of the vessel, to the surface zone (<2-cm depth; >30% of surface PAR). A cell moved into the surface zone with an average frequency of 0.17 s^{-1}, or one transition every 6 s. The average surface event lasted for only 0.7 s, and the average time a cell went into the lower half of the ePBR (<1.5% of surface PAR) was 2.6 s. The maximum length of a surface event that happened at least every hour was 6 s, whereas dark events with a length between 6 and 12 s occurred every 7 min on average.

We integrated the vertical-mixing light model with the diurnal change in surface light intensity. This illustrated how the cell-specific light environment is highly dynamic across the day (Fig. 4). We report all sampling times as ZT, which is commonly used in circadian rhythm studies, with dawn representing ZT0 (McClung, 2006). At ZT6 (6 h past dawn, light flux zenith), the model predicted that the 10-min average cell-specific light exposure was approximately 300 μmol photons m^{-2} s^{-1}. This included brief exposures to irradiances up to 2,000 μmol photons m^{-2} s^{-1} as cells reached the surface (Fig. 4D). Across the whole day, our model estimated that cells would experience around 10%–15% of the surface PAR when averaged across a 10-min period (Fig. 4D). When we integrated the light environment across the full 12-h light period of the day, the cell-specific photon flux was 180 μmol photons m^{-2} s^{-1}.

We grew *Synechocystis* at a constant light flux of 180 μmol photons m^{-2} s^{-1} in 12-h light:12-h dark conditions as dilute cultures in Erlenmeyer flasks. We found that these cultures grew 10 times faster than what we observed in the ePBR (7.9 ± 0.7 versus 75 ± 22 h; Supplemental Fig. S1). This suggests that the rapidly changing light environment causes a major reduction in the capacity of *Synechocystis* to utilize photons efficiently for growth.

The spectral composition in light at a specific depth in the culture did not change until below 2-cm depth (Supplemental Fig. S5), at which point 75% of the light had already been absorbed (Fig. 4A). We assumed that the change in the spectrum of light as it penetrates the culture likely has a negligible effect on the overall photosynthetic rates of the culture.

Diurnal Changes in Biovolume and Pigmentation

We measured changes in cell size, division rate, and pigment composition across the day. The cell population displayed a small, but statistically significant, change in the average size across the day, ranging

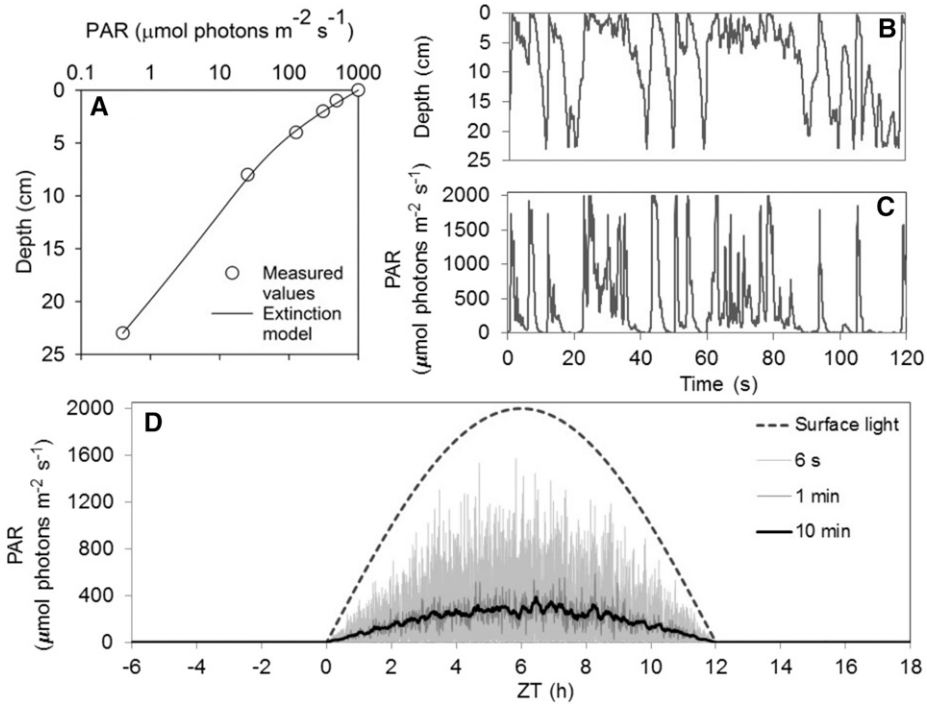

Figure 4. Diurnal changes in the cell-specific light environment. A, Light extinction through the ePBR vessel measured at six discreet depths and modeled based on Equation 3. B, CFD results showing the vertical position of a single cell in the ePBR during 2 min. C, The vertical position in C translated to the cell-specific light environment using the surface light intensity at Zeitgeber time 6 (ZT6) and the light extinction model shown in A. D, The cell-specific light environment model across a day, including diurnal changes in surface light intensity. For clarity, only running averages of 6 s, 1 min, and 10 min are shown. PAR, Photosynthetically active radiation.

between 1.5 and 1.7 μm^3 ($F_{12,60}$ = 116, $P < 0.001$; Fig. 5A). Cell size appeared to increase in the morning, and by ZT3 the average cell was significantly larger than at ZT0 (see Supplemental Table S1 for detailed statistical results). Overall, the cells had a cell volume about 3 times smaller than those grown in constant high light (Supplemental Table S2).

An important acclimatization response to shifting light intensities in cyanobacteria is modification to the pigment composition and light-harvesting capacity (MacIntyre et al., 2002). In our experiments, chl *a* content per unit biovolume did not change significantly in the ePBR culture at any point during the day ($F_{12,59}$ = 1.11, P = 0.366; Fig. 5B), and chl *a* was maintained around 12 fg chl *a* [μm^3 biovolume]$^{-1}$. The chlorophyll content was similar to low-light-acclimatized cells (16.1 ± 3.3 fg chl *a* [μm^3 biovolume]$^{-1}$; Supplemental Table S2). There was a minor, but statistically significant, diurnal modification in the total carotenoid:chl *a* ratio, which covaries with the sinusoidal change in surface irradiance, albeit skewed toward the morning ($F_{12,59}$ = 38.5, $P < 0.001$; Fig. 5C).

Diurnal Changes in TOC and Nitrogen Content

The cell-specific TOC content changed in a sinusoidal pattern following the illumination and closely resembled the changes in biovolume (Fig. 5D). The TOC content was significantly larger between ZT3 and ZT11.75 than at other times of day ($P < 0.001$; Supplemental Table S1), and at ZT6 the TOC content peaked at 0.65 pg TOC cell^{-1} ($F_{12,60}$ = 4.521, $P < 0.001$; Fig. 5D). The ratio of TOC to total cellular nitrogen did not change on a diurnal basis and was maintained at 5.1 ± 0.5 (n = 68). The diurnal changes in carbon content were integrated with the cell division rate to observe that the culture accumulated 3.5 ± 0.1 mg TOC L^{-1} h^{-1} during the daytime ($F_{2,10}$ = 26.6, $P < 0.001$; Fig. 5E). Across the whole illumination period, the productivity of the culture was 35 ± 3 mg TOC L^{-1} day^{-1} or 9.0 ± 0.7 g TOC m^{-2} day^{-1} when normalized to the surface area of the reactor. There was a small, although statistically significant, reduction in the average TOC content per cell at night (Fig. 5E).

Diurnal Changes in Photosynthetic Physiology

We observed no change in the shape of photosynthesis-irradiance (P-I) curves measured ex situ over the course of the day (Fig. 6A). Correspondingly, there were no statistically significant changes in photosynthetic parameters associated with the P-I curve (Table 1). This

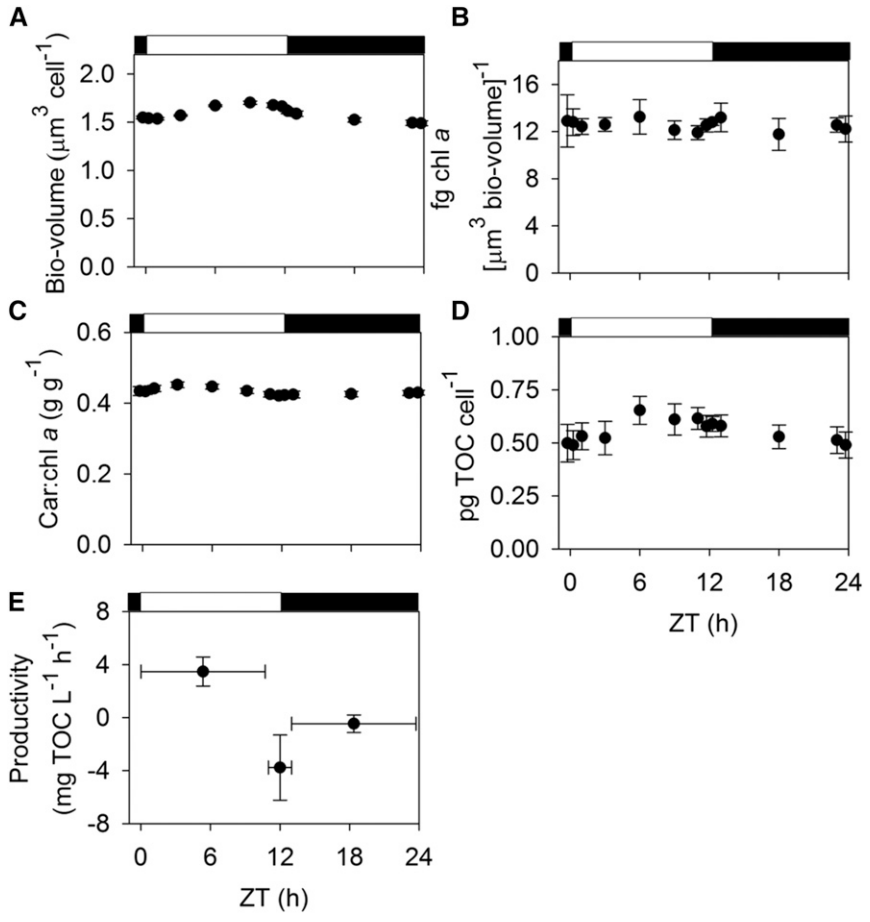

Figure 5. Diurnal changes in cellular properties. A, Average biovolume of cells. B, Chlorophyll *a* (chl *a*) density per biovolume. C, Total carotenoid:chl *a* ratio (Car:chl *a*). D, Cell-specific total organic carbon (TOC) content. E, Productivity described as TOC accumulation per volume culture. Differences between time points were analyzed using repeated-measurement ANOVA (RM-ANOVA; n = 5–6). For clarity, we have provided results from the statistical analysis between time points in a separate table (Supplemental Table S1). Vertical error bars = SD (n = 5–6); horizontal bars = temporal range encompassed in the averages (E).

suggests that a robust photosynthetic rate was maintained regardless of surface light intensities. The chl *a*–normalized maximum rate of photosynthesis, P_{max}, ranged from 469 to 527 μmol O_2 (mg chl *a*)$^{-1}$ h^{-1}, and the saturation index (E_k) ranged from 341 to 429 μmol photons m^{-2} s^{-1} (Table 1). Since we observed no statistical changes in the P-I parameters, we pooled all measurements (15 response curves and 210 individual measuring points) and defined the saturation point of photosynthesis ($P_{half\text{-}max}$) and the optimum irradiance for photosynthesis ($E_{optimum}$) using the wait-in-line model (Ritchie and Larkum, 2012). $P_{half\text{-}max}$ was reached at 250 μmol photons m^{-2} s^{-1}, whereas the optimal irradiance for photosynthesis, $E_{optimum}$, occurred at 1,050 μmol photons m^{-2} s^{-1}.

NPQ in *Synechocystis* is a complex interaction between state transitions, OCP-dependent quenching (OCP-quenching), and various other quenching mechanisms (Kirilovsky, 2015). Fluorescence changes monitored during our ex situ P-I curves under white light suggested an initial level of fluorescence quenching, which was most likely state transition related given the low light intensities (<50 μmol photons m^{-2} s^{-1}), followed by OCP-quenching induction, initiated at around 350 μmol photons m^{-2} s^{-1} (Fig. 6B).

We also estimated the maximum capacity for OCP-mediated NPQ as induced through the application of 7 min of strong blue light (880 μmol photons m^{-2} s^{-1}). The maximum NPQ capacity was significantly higher in the morning (ZT1 and ZT3; 0.48 and 0.43) than midday or the afternoon (0.41 and 0.41; $P < 0.001$; Table 2). The F_M' did not fully recover under subsequent dim blue light illumination (residual quenching: 9.0% ± 0.5%, $n = 14$), suggesting that state transition, photodamage, and/or an OCP-independent mechanism may have contributed to the maximal quenching (Supplemental Fig. S6). Due to the rapid induction and reversion of state transitions, this parameter cannot be measured in situ using our methodology, but the capacity for state transitions ex situ was significantly higher at ZT1 than midday or the afternoon ($P < 0.001$; Table 2). Contrastingly, the level of in situ OCP-quenching in the ePBR culture was very low across the day (<0.02 × quenching of F_M) and did not change significantly on a diurnal basis ($P = 0.073$; Table 2). Collectively, these results show that the cells did have OCP-related NPQ capacity, but it was not significantly active in situ across the day.

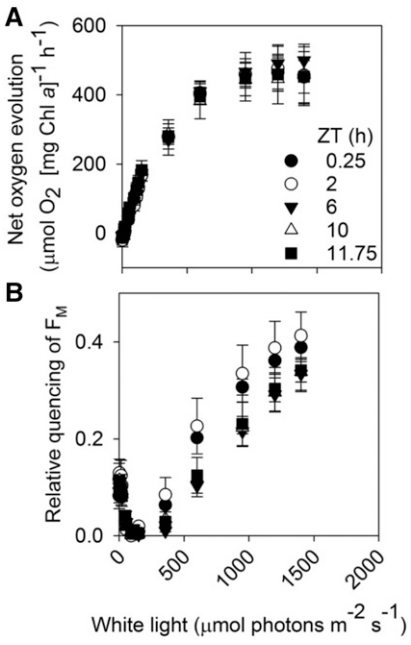

Figure 6. P-I curves. A, Net oxygen production measured with a oxygen probe (FireSting). B, Relative quenching of fluorescence versus irradiance. The white light-emitting diode (LED) growth lights of the ePBR were used as an actinic light source. Shown are averages ± SD ($n = 3$; and averages and range ($n = 2$; B). Chl *a* concentration was 3.0 ± 0.5 μg mL^{-1} during the measurements.

The in situ maximal quantum yield of PSII (F_v/F_M) varied between 0.45 and 0.52 throughout the day (Fig. 7). There was a pronounced increase/decrease in F_v/F_M during the transition from dark to light and from light to dark (Fig. 7), from about 0.48 to 0.53. There was also a small, but statistically significant, reduction in F_v/F_M around the peak surface light intensity (from 0.53 to 0.50 at ZT6 and ZT9, respectfully).

Quantitative Integration of Photophysiology and Light Fluxes

We integrated our measurements of the photosynthetic parameters with the cell-specific light exposure model to illustrate how the cell-specific light environment of the ePBR can be expected to affect photosynthesis (Fig. 8A). Summed across the illuminated part of the day, the cells spent more than half the time at light intensities below the compensation point of photosynthesis (net respiration). Only one-third of the day was spent at light intensities within the linear response range of photosynthesis (>compensation point, <$P_{half\text{-}max}$), and less than 30 min of the day was at suprasaturating light intensities (>$E_{optimum}$; Fig. 8A). Interestingly, this 30 min of suprasaturating light exposure (>1,050 μmol photons m^{-2} s^{-1}) supplied the cells with ~40% of their daily photon flux (Fig. 8B). These saturating light pulses were also supplied in <1-s pulses (Fig. 4; Supplemental Fig. S4A). Another ~40% of the integrated photon flux was supplied in the nonlinear response range (>$P_{max\text{-}half}$, <$E_{optimum}$).

Effects of Fluctuating Light on Oxygen Evolution and Consumption Ex Situ

To investigate the activity of photoprotective mechanisms under fluctuating light, we programed the DUAL-PAM fluorometer's actinic light to replicate the modeled cell-specific light environment of the ePBR. A combination of two-part red (654 nm) and one-part blue (430 nm)

Table 1. *Parameters derived from the rapid P-I curves*

Differences between time points were analyzed using one-way RM-ANOVA ($n = 3$) and were not significantly different for any of the five parameters.

	P-I Parameters on Chl *a* Basis				
ZT (h)	Dark Respiration (μmol O_2 [mg chl *a*] h^{-1})	Compensation Point (μmol photons m^{-2} s^{-1})	α (μmol O_2 [mg chl *a*] h^{-1})/ (μmol photons m^{-2} s^{-1})	P_{max} (μmol O_2 [mg chl *a*] h^{-1})	E_k (μmol photons m^{-2} s^{-1})
0.25	−17.1 ± 8.6	11.7 ± 6.50	1.29 ± 0.15	482 ± 68	374 ± 62
2	−19.1 ± 8.6	9.32 ± 8.32	1.22 ± 0.17	483 ± 64	403 ± 105
6	−15.7 ± 8.6	9.33 ± 6.03	1.23 ± 0.05	527 ± 17	429 ± 31
10	−14.5 ± 9.9	6.33 ± 7.77	1.31 ± 0.17	467 ± 64	363 ± 89
11.75	−18.8 ± 10.5	9.00 ± 9.50	1.42 ± 0.26	469 ± 32	341 ± 88
$F_{4,8}$ (p)	0.138 (0.963)	0.311 (0.863)	1.29 (0.352)	1.29 (0.352)	2.87 (0.095)

light was used to mimic the light environment in the ePBR at various time points throughout the day (e.g., 200 μmol photons m^{-2} s^{-1} red light would be supplied with 100 μmol photons m^{-2} s^{-1} blue light). We generated a 5-min fluctuation light schedule that was looped during measurements (Supplemental Fig. S7). Using ePBR-acclimatized cultures, we measured chlorophyll fluorescence as well as simultaneous oxygen production and consumption rates during the treatment via membrane inlet mass spectrometry (MIMS). At ZT0.25, the maximum light intensity was 130 μmol photons m^{-2} s^{-1} with long periods of darkness and an integrated photon flux of 18 μmol photons m^{-2} s^{-1}. At noon, the treatment peaked at a maximum light intensity of 2,000 μmol photons m^{-2} s^{-1} and an integrated photon flux of 284 μmol photons m^{-2} s^{-1} (see Supplemental Table S3).

Observations of DUAL-PAM fluorescence traces showed some initial quenching of F_M in the first few minutes of fluctuating actinic light (Fig. 9). After that, a repetitive pattern in F_M' emerged between the 5-min loops during the rest of the treatment, with lower values during dark-dominated periods and higher values during a series of rapid light flashes (Fig. 9). Given the rapid, but small, changes in F_M', this was most likely due to continuous state transitions and not OCP-mediated NPQ. The Y(II) oscillated between 0 and 0.2 and could indicate the majority of PSII reaction centers shifted between open and closed in the rapidly changing light regime (Fig. 9). We note that a red measuring light was used to measure fluorescence in these experiments, and values likely represent fluorescence from both PSII and phycobilisomes (Acuña et al., 2016). Additionally, respiratory electron flow in cyanobacteria can cause underestimation of true Y(II), so these measurements should be interpreted with caution (Schuurmans et al., 2015).

The ex situ fluctuating light treatment caused profound alterations to oxygen fluxes based on simultaneous measurements of illuminated oxygen evolution and consumption using MIMS. Oxygen evolution peaked at ZT6 (212 ± 19 μmol O_2 [mg chl *a*]$^{-1}$ h^{-1}; Fig. 10A). The rate of light-dependent oxygen consumption increased from –25 ± 5 to –106 ± 15 μmol O_2 [mg chl *a*]$^{-1}$ h^{-1} between ZT0.25 and ZT6 (Fig. 10B). Light-dependent oxygen consumption rates were higher than dark respiration (–15 to –20 μmol O_2 [mg chl *a*]$^{-1}$ h^{-1}; Table 1), indicating that the light-dependent oxygen consumption was due to light-induced AET. It appeared that the high light intensities during the brief flashes of light were not the sole driver of light-dependent oxygen consumption, since both static and fluctuating light yielded similar rates of light-dependent oxygen consumption in the same biological replicate (Supplemental Fig. S8).

Between ZT2 and ZT10, when cells are supplied with the majority of photons, light-dependent oxygen consumption accounted for ~50% of the electrons passing through the electron transport chain, reducing net photosynthesis to <106 μmol O_2 (mg chl *a*)$^{-1}$ h^{-1} (Fig. 10C). Consequently, net photosynthesis only reached 20% that

Table 2. *Relative quenching of maximum fluorescence and its origin*

A Walz DUAL-PAM fluorometer with a red measuring light (620 nm) and blue actinic light (430 nm) was used to derive in situ capacities for fluorescence quenching. Data are shown as relative quenching of maximum fluorescence. Differences between time points were analyzed using one-way RM-ANOVA ($n = 3$). Letters denote significant differences between time points ($P < 0.05$).

ZT Time (h Past Dawn)	In Situ OCP ($OCP_{in\ situ}$)-Quenching	Maximal OCP Capacity (OCP_{max})-Quenching	State Transition Quenching Capacity (State-Quenching)
1	0.00 ± 0.00	0.484 ± 0.014 a	0.274 ± 0.035 a
3	0.020 ± 0.010	0.433 ± 0.016 a,b,c	0.240 ± 0.021 a,b
6	0.015 ± 0.011	0.408 ± 0.015 b,c	0.223 ± 0.020 b
9	0.010 ± 0.001	0.411 ± 0.013 c	0.230 ± 0.013 b
11	0.011 ± 0.003	0.408 ± 0.013 c	0.234 ± 0.011 b
$F_{4,8}$ (p)	3.25 (0.073)	10.6 (0.003)	9.58 (0.004)

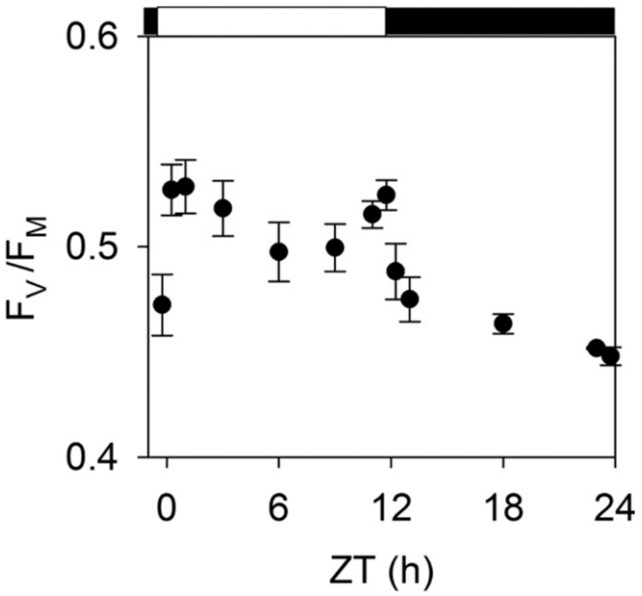

Figure 7. In situ F_v/F_M measured using a blue excitation light (450 nm). Shown are averages ± SD ($n = 3$). Differences between time points were analyzed using RM-ANOVA ($F_{12,47} = 45.5$, $P < 0.001$). Results from the statistical analysis between time points are shown in a separate table (Supplemental Table S1).

of the maximum capacity (P_{max}) of the culture (482 ± 68 μmol O_2 [mg chl *a*]$^{-1}$ h^{-1}; Table 1). In the early morning and evening, an even greater proportion of electrons were diverted to oxygen, maintaining net photosynthesis close to the compensation point. Together, these ex situ results suggest that a combination of light-induced AET and an inability to efficiently harvest photons during the brief (~1 s) suprasaturating light flashes reduces the photosynthetic efficiency of *Synechocystis* in the ePBR.

DISCUSSION

For aquatic photoautotrophs, their light environment changes throughout the day because of diurnal changes in solar irradiance, weather phenomena, and mixing from surface waters to depth. The changes associated with mixing can be exacerbated when the environment is particularly turbid, such as in a coastal algal bloom or during industrial cultivation. Our goal for this study was to create a framework that first develops detailed mixing models, translates this mixing to changes in the light regime, and then applies this light model to investigate the responses of photosynthetic physiology to this complex environment.

The Use of CFD to Model PBRs

Many investigators have applied numerical modeling to characterize different aspects of PBR operation and performance, including mixing efficiency, cell growth rates, light penetration, gas and cell motion, and energy requirements. Of the different modeling strategies, CFD has been the most common approach to capture the physics and biology of fluid motion, mass transport, cell growth kinetics, and light transmission within the various types of PBRs (Bitog et al., 2011). The studies differ from one another based on the specific bioreactor geometry and information to be extracted from the predictions, as well as how the light source is introduced, and together these dictate model complexity and computational requirements.

Although commercial CFD packages such as COMSOL (www.comsol.com) and ANSYS (www.ansys.com) Fluent are continuously refined and massively parallel computing systems are readily available, even recent CFD studies have made simplifying assumptions for the sake of computational tractability. In some cases, full three-dimensionality is achieved by assuming the flow is laminar and simpler to simulate (Kayahan et al., 2016). However, even when more realistic flow conditions are modeled, other simplifying geometric assumptions are made, such as treating an airlift column PBR as two-dimensional (Calvo et al., 2017), or assuming axisymmetric conditions in a Taylor vortex PBR

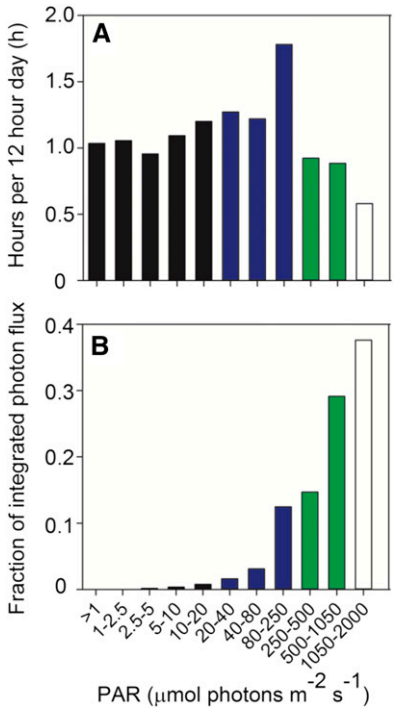

Figure 8. Integration of the cell-specific light environment with P-I parameters. A, Accumulation of time a cell was predicted to spend at different light intensities throughout the day. B, Fraction of integrated daily photon flux cells receive at each light intensity. Categories are based on pooled analysis of all diurnal P-I curves ($n = 15$ response curves and 210 data points) using the wait-in-line model as described by Ritchie (2008). Black bars, time spent below the compensation point; blue bars, time spent in the linear response range ($< P_{half\text{-}max}$); green bars, time spent in the nonlinear response range ($> P_{half\text{-}max}$; $< E_{optimum}$); and white bars, time spent in saturation ($> E_{optimum}$).

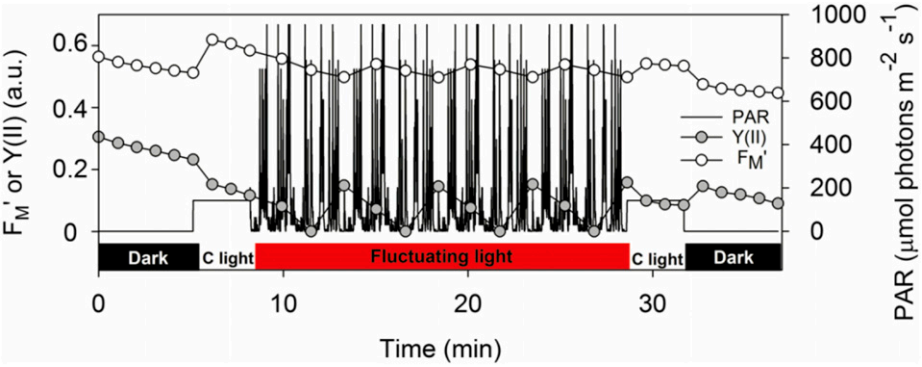

Figure 9. Chlorophyll fluorescence during the ex situ fluctuating light treatment. Example of a representative sample at ZT2. Maximal fluorescence (F_M') and the yield of PSII, Y(II), is shown along with the changes in light intensity across the treatment (PAR line). Saturating pulses were applied every 60 s during constant L/D and every 100 s during fluctuating light. C light, Constant light. Chl *a* concentration was 15 μg mL^{-1}. a.u., arbitrary units.

(Gao et al., 2017). The other common simplifying constraints are the assumption of steady-state conditions (Soman and Shastri, 2015), which is not realistic in turbulent flow, or prescribing a constant bubble size and shape (Huang et al., 2016). In this work, none of these simplifying assumptions were exercised. The simulations were fully three-dimensional. The fluid and bubble motion were treated as turbulent and time dependent, the gas phase was injected at a specified flow rate, and bubbles formed, coalesced, broke apart, and deformed as they rose. This study is by no means the first to apply the aforementioned level of rigor but it is notable for its lack of simplifying assumptions.

Mixing Dynamics Approximate Tubular PBRs

Previous studies have focused on the response of algae/cyanobacteria in the photic zone of the open ocean (slow mixing and low turbidity, e.g., Dimier et al., 2009) or strove to improve productivity in industrial scenarios (e.g. Huang et al., 2014; Park and Li, 2015). We believe the approach presented here allows for the additional ability to understand more about how photophysiology and cellular biochemistries respond to rapidly changing light.

One of our experimental objectives was to generate and describe a light regime similar to that found in closed industrial PBRs. We used the Phenometrics ePBR, which was originally designed to mimic a raceway pond in terms of depth and illumination (Lucker et al., 2014). However, we operated the ePBR differently than the original authors, who allowed only brief bursts of mixing every 10 to 15 min. In contrast, we mixed and sparged the ePBR continuously to generate a rapid mixing regime that more closely resembles closed tubular or airlift PBRs (Posten, 2009). This moved cells in and out of the illuminated region of the ePBR with an average frequency of 0.17 s^{-1} (Fig. 4), comparable to reports for industrial-scale tubular and airlift PBRs (10–0.01 s^{-1}; Perner-Nochta and Posten, 2007; Huang et al., 2015). Most PBRs are designed with a cross section that is only a few centimeters thick, whereas the ePBR is 25 cm deep. Thus, the surface-to-volume ratios of PBRs are generally ~50 m^{-1} (Posten, 2009), whereas the ePBR has a ratio of only 7.5 m^{-1}. As a result, significantly less light would penetrate our total culture volume if our ePBRs were run at the same cell density as an industrial PBR. Because of this, we used an experimental cell density more dilute than that found in industrial PBRs. Our culture density was approximately 0.15 g dry weight L^{-1} (based on 0.08 ± 0.01 g TOC L^{-1} with 50% of the total biomass consisting of carbon; Kim et al., 2011). This is considerably less than what is typically used in tubular PBRs (1–10 g dry weight L^{-1}; Brennan and Owende, 2010), but it did allow for some light penetration into the culture (Fig. 4).

The conditions used for our study appear to adequately imitate an industrial-scale PBR as assayed by culture growth and productivity. We observed surface area–normalized biomass accumulation rates of 9 g TOC m^{-2} day^{-1} (18 g dry weight m^{-2} day^{-1}), which is within the range reported for various closed PBRs (10–40 g dry weight m^{-2} day^{-1}; Brennan and Owende, 2010). Additionally, the cell division rates of the semicontinuous cultures used in our experiments (~3 d) resembled rates reported for algae and cyanobacteria in PBR field experiments (doubling times ranging between 1 and 10 d; Brennan and Owende, 2010). Although the range of conditions in industrial-size PBRs are highly variable, these data suggest the ePBR system can facilitate characterization of *Synechocystis* photophysiology under industrially relevant conditions.

Modeling the Dynamics of Light Change over a Day

Previous studies have applied CFD to describe and understand the mixing of cells within a PBR. The CFD model from this study predicted that individual cells in our ePBR treatment were subjected to a time-integrated photon flux of 180 μmol photons m^{-2} s^{-1} throughout the day. The cell-specific light model showed that 6 h out of the 12-h day period was spent below the compensation point for photosynthesis (Fig. 8). Only a combined 2.5 h per daytime was spent above the $P_{\text{half-max}}$ (250 μmol photons m^{-2} s^{-1}), where photosynthesis operates at a high rate. This light was delivered to the cells as a few thousand flashes with a duration often less than 1 s during the day (Fig. 4C). This is likely not enough time to sustain metabolic processes across the relatively long periods (1–6 s) spent below the compensation point.

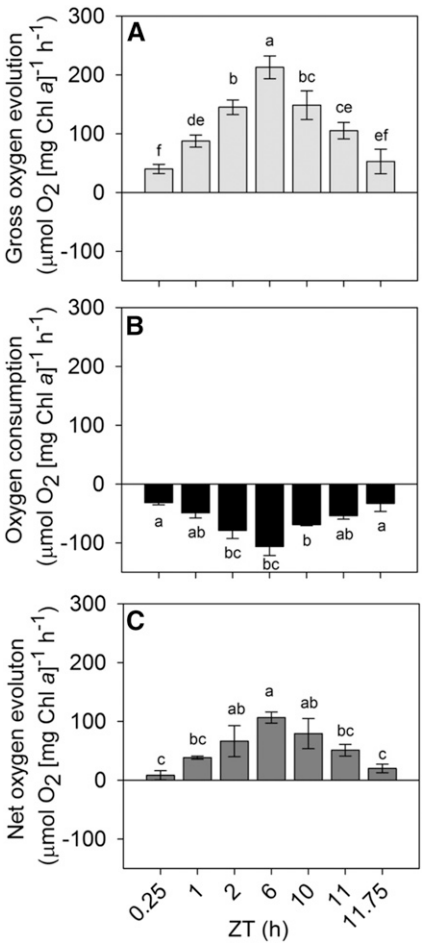

Figure 10. Illuminated rates of oxygen evolution and consumption during the ex situ fluctuating light experiment. The light treatment was based on to the cell-specific light environment model, applied using a mixture of blue (430 nm) and red (640 nm) LEDs of the DUAL-PAM, and measurements were collected using MIMS. See Supplemental Table S3 for information on maximum and integrated photon flux at different ZT times. A, Gross oxygen evolution corresponding to photosynthesis. B, Light-dependent oxygen consumption corresponding to respiration and alternative electron transport (AET). C, Net oxygen evolution (evolution + consumption). Temporal differences in evolution, consumption, and net photosynthesis were analyzed using one-way RM-ANOVA with $F_{6,12} = 34.6$, 21.0, and 14.3, respectively, and $P < 0.001$ for all three parameters. Letters a–f indicate statistically significant differences. Chl *a* concentration was 15 μg mL^{-1}. Shown are averages ± SD ($n = 3$).

Our CFD model illustrates the stochastic and dynamic light environment experienced by cells in PBRs. Yet the effect of rapidly fluctuating light on photosynthesis has mainly been investigated through highly controlled L/D flash experiments using square-wave treatments of suprasaturating (500–2,000 μmol photons m^{-2} s^{-1}) monochromatic light. These studies have shown that at L/D oscillation of ~100 s^{-1}, growth rates are maintained or are slightly elevated compared to constant light (Nedbal et al., 1996). The elevated growth rates were presumed to be due to reductions in photodamage. On the other hand, slow square-wave L/D oscillations >0.1 s^{-1} have been proposed to have a positive impact on culture productivity by allowing regeneration of essential metabolites downstream of the electron transport chain during dark periods (Takache et al., 2015). Additionally, growth rates of algae in scaled-down PBRs correlate with the frequency of L/D oscillations under static surface light (Huang et al., 2015). However, as the frequency of L/D oscillations decrease below 0.1 s^{-1}, there appears to be little effect on the growth of autotrophic cultures. Instead, growth rates shift to correlate with surface intensity or duration of the light period (Barbosa et al., 2003). We note that these studies did not include diurnal fluctuations in light associated with outdoor conditions.

Our light model suggested that the *Synechocystis* cultures received an average of 180 μmol photons m^{-2} s^{-1} over the course of the day. If supplied as static light in dilute cultures, this flux is predicted to saturate growth of *Synechocystis* (Du et al., 2016). Indeed, we observed that cultures grown under static light of the same integrated photon flux as in the ePBR (12/12 h, 180 μmol photons m^{-2} s^{-1}/dark) grew 10 times faster than ePBR cultures (Supplemental Fig. S1). We performed an additional experiment to verify that fluctuating light lead to low growth rates in dense culture. We grew cells at low densities (inoculated in the range of 130–260 × 10^3 cells/ml) and programmed the ePBR lights to fluctuate in 1-s intervals that mimicked our modeled light fluxes in dense culture across the day (Supplemental Fig. S9). Doubling time for these cultures was 94 ± 19 h ($n = 3$), which is within the range seen for our dense cultures (Fig. 1). Conversely, cells grown in a square-wave light regime of 177 μmol photons m^{-2} s^{-1} incident light had a doubling time of 12 ± 4 h ($n = 3$). Therefore, the irregular supply of photons in a rapidly fluctuating light environment has a profound negative impact on the capacity of *Synechocystis* to utilize photons efficiently to support growth and biomass accumulation. Our results suggest that the previously observed boosts in productivity associated with flashing light (see previous paragraph) may be an artifact of controlled laboratory conditions and is not applicable to current state-of-the-art PBRs grown under natural light conditions. Our observations also indicate that slow growth in our culture conditions is not likely due to nutrient limitation or any potential cell-cell interactions that could slow growth (Esteves-Ferreira et al., 2017).

Diurnal Changes in Photosynthetic Capacity

The photosynthetic capacity of the ePBR culture, according to our ex situ P-I curves, was robust across the day (Fig. 6; Table 1). Interestingly, the TOC-normalized P_{max} was twice as high in the ePBR culture compared to exponentially growing cells under both static low or high light (30 and 400 μmol photons m^{-2} s^{-1}; Supplemental Table S4). Such an elevated P_{max} suggests that the ePBR culture had optimized the capacity to process electrons downstream of PSI

(Behrenfeld et al., 2004), likely in an effort to maximize the utilization of photons harvested during the intense but brief flashes (Yarnold et al., 2016). We sought to better understand the fate of absorbed light energy using a series of PSII fluorescence and gas exchange measurements.

There appeared to be very little accumulated damage to PSII. We used a blue measuring light to investigate the F_v/F_M, and our results (0.53–0.50 during the illuminated period) are within the range reported for other cyanobacteria species that have been probed with a blue measuring light under nutrient-replete conditions and low light intensities (Ritchie, 2008; Liu and Qiu, 2012). This suggests that very little, if any, photoinhibition to PSII occurred in situ in the ePBR. Our observations of F_v/F_M stand in contrast to observations in the green algae *Chlamydomonas reinhardtii*, where 0.1 s^{-1} simulated L/D oscillation in excess light caused photodamage and reduced growth rates (Yarnold et al., 2016). This difference may be explained by the fact that an individual cell in our study only spent a total of 30 min per 12-h day period in excess light. This may not be sufficient time to cause major photodamage and/or it provides ample time in the dark to permit recovery/repair mechanisms to fix damaged PSII. The sharp increase/decrease in F_v/F_M around dawn and dusk (Fig. 6) likely coincides with state transitions (Behrenfeld and Kolber, 1999). Our ex situ P-I curves also suggested that there was no significant photodamage, as photophysiological parameters calculated did not change throughout the day (Fig. 6; Table 1). Overall, these results suggest a robust photosynthetic apparatus in the ePBR.

Diurnal Changes in NPQ

NPQ is one mechanism used by autotrophs to harmlessly dissipate energy when photons are absorbed in excess of their photosynthetic capacity. The NPQ mechanism is often suggested to be important under light conditions associated with mass cultivation. Tuning NPQ directly, or indirectly through reduction of the antenna size, has been suggested as an avenue of genetic engineering toward high productivity strains (Melis, 2009; Peers, 2014; Berteotti et al., 2016). Interestingly, there have been few actual measurements of NPQ in situ in PBRs. Measurements that are published are primarily based on P-I curves and thus capture the NPQ capacity and not the in situ activity (Masojidek et al., 2003; Berteotti et al., 2016; Yarnold et al., 2016).

In this discussion, we distinguish between fluorescence parameters collected using red or blue measuring lights on the DUAL-PAM, since the former excites phycobilisomes and chl *a*, whereas the latter only targets chl *a*. This has important impacts on the amplitude of the F_v/F_M parameters and abilities to detect phycobilisome-related quenching mechanisms such as state transitions and OCP-quenching (Acuña et al., 2016).

We observed that OCP-dependent NPQ in the ePBR-acclimatized culture was not induced in our ex situ P-I curves until ~300–500 μmol photons m^{-2} s^{-1} (Fig. 6B). We used the red measuring light of the DUAL-PAM to detect OCP-dependent NPQ, which occurs at the level of the phycobilisome. The white LED of the ePBR was used as actinic light to better mimic in situ conditions. Given that the predicted 10-min average cell-specific photon flux was never above 400 μmol photons m^{-2} s^{-1} in the ePBR (Fig. 4C), we would expect that at any given time, only a very small fraction of cells would induce OCP-quenching in situ. Additionally, a larger portion of the blue light, which activates OCP-dependent quenching, is nearly absent by 2-cm depth and below (Supplemental Fig. S5). This reduces the likelihood that NPQ is induced in any given cell. Importantly, we could not detect significant NPQ induction at any point throughout the day when we estimated in situ quenching of fluorescence within the ePBR culture (utilizing red measuring light; Table 2). These results suggest that NPQ is not an important process for dissipating excess energy in our experimental conditions.

The regulation of rapidly inducible NPQ is very different between cyanobacteria and microalgae or plants with a light harvesting complex–based NPQ. Chloroplast containing eukaryotes regulates NPQ through acidification of the lumen (Erickson et al., 2015), whereas OCP acts as a dual photoreceptor/quencher and blue light intensity induces its quenching capacity (Wilson et al., 2006). It is possible that other cyanobacterial or microalgal species induce NPQ at lower light intensities, and depending on the design of the reactor, the irradiance threshold for NPQ may be reached at some point throughout the day. We have previously observed that disruption of OCP increased growth rates of *Synechocystis* in thin PBRs in greenhouses (Peers, 2015), suggesting that NPQ induction will occur if the integrated light intensities are high enough. On the other hand, we did not observe induction of NPQ in situ in the ePBR using the model diatom *Phaeodactylum tricornutum* (Jallet et al., 2016a). These contrasting observations collectively illustrate that it cannot be simply assumed that NPQ is induced under rapidly fluctuating light.

Diurnal Changes in AET

We used MIMS to measure oxygen consumption and evolution ex situ using the cell-specific light environment predicted from our CFD model. Unfortunately, the white LED of the ePBR could not be programed to respond quickly and accurately enough to recreate the cell-specific light environment ex situ. We used the dichromatic actinic light (654 and 430 nm) of the DUAL-PAM fluorometer to mimic the fluctuating light output of the model. These two wavelengths specifically target the peak absorption of chl *a* and phycobiliproteins (Supplemental Fig. S10) and, therefore, drive photosynthesis more efficiently than the white light of the ePBR does ($\alpha = 1.23 \pm 0.05$ compared to 3.72 ± 0.27 for the white LEDs of the ePBR; Supplemental Table S5). So, we caution the reader that the measured rates of

oxygen fluxes may be overestimated compared to those seen in the ePBR.

We observed light-induced oxygen consumption, or AET, when we subjected ePBR cultures to the predicted cell-specific light environment ex situ. Based on the MIMS quantification, light-dependent oxygen consumption dispensed approximately 50% of the electrons flowing through the electron transport chain. This is a similar amount relative to what has been observed under highly stressful conditions such as carbon limitation and for minute-scale fluctuations in growth light (Allahverdiyeva et al., 2013; Shimakawa et al., 2015; Ermakova et al., 2016).

AET is an important photoprotective mechanism in cyanobacteria (Ermakova et al., 2016). Under regularly fluctuating, square-wave light conditions, mutants of *Synechocystis* sp. PCC 6803 lacking either of the photoprotective flv heterodimers (Flv2/4 and Flv1/3) or the cytochrome *bd* quinol oxidase experience severely reduced growth phenotypes and photobleaching (Zhang et al., 2012; Allahverdiyeva et al., 2013; Lea-Smith et al., 2013). In combination with our results, this suggests that AET, and not NPQ, is the primary photoprotective mechanism used by *Synechocystis* sp. during growth in fluctuating light. By using AET instead of NPQ, the cells also have the potential benefit of creating a proton motive force that can be used to generate ATP for biochemistry that does not require NADPH, such as transporter activity (Kramer and Evans, 2011).

Very little is known about what regulates mechanisms of AET. The redox state of the plastoquinone pool exerts a strong influence on global transcription (Hihara et al., 2003) and regulates NPQ in plant chloroplasts (Oxborough and Horton, 1988), so it may influence the activity of AET, too. Our experimental conditions frequently exposed cells to several seconds of light intensities below the compensation point for photosynthesis. This likely leads to rapid oxidation of the plastoquinone pool, as suggested by the fluctuations in Y(II) (Fig. 9), which could induce transcription of genes associated with respiration or activation of terminal respiratory oxidases. Conversely, transcripts associated with photoprotective processes are accumulated during excess light (Hihara et al., 2001). Perhaps short pulses of excess light would reduce the plastoquinone pool that could lead to the activation of enzymes involved in photoprotective AET. We cannot pinpoint the enzymes involved in AET with our physiological data. Regardless of the mechanism, downregulating AET through genetic manipulation may be a successful way to divert more electrons toward NADPH production and increase carbon fixation and growth of *Synechocystis* in PBRs with rapid mixing and thin optical path lengths.

CONCLUSIONS

We aimed to develop a framework to better understand the response of photosynthetic microbes to rapid mixing conditions. We isolated the effects of dynamic and rapidly changing light and showed that it did not induce NPQ in situ, and there was no indication of photoinhibition in *Synechocystis* sp. PCC 6803. This result stands in contrast to common perceptions that the light environment in PBRs inevitably induces excess NPQ and causes photodamage in PBRs (Posten, 2009; Kirst et al., 2014). Much of our understanding of high light stress and photoacclimatization in algae and cyanobacteria comes from experiments where cells are acclimatized to low light intensities for dozens of generations and suddenly subjected to high light (e.g. Hihara et al., 2001). This may not reflect long-term photoacclimatization to growth in PBRs or in natural conditions. If our results extend to other species and scaled PBRs, it indicates that attempts at tuning NPQ through genetic engineering may have little effect on the productivity of the PBR. Attempts at reducing photodamage through reactor design, rapid fluctuations in light, or genetic engineering may also be misguided efforts. Instead, our data suggest that more focus should be placed on exploring whether AET can be manipulated to increase productivity of algae or cyanobacteria in industrially scaled PBRs.

In mass cultivation conditions with less fluctuating light, such as thin PBRs or less dense cultures, it is still possible that NPQ can be targeted to increase productivity. The discrepancies between different studies may be solved through better models and observations of cell-specific light histories in commercial state-of-the-art PBRs. Future strain engineering attempts should be evaluated against a given benchmarked light environment. In situ measurements of NPQ in wild-type strain should also accompany these engineering attempts to illustrate the feasibility of the approach.

In this study, we characterized the cell-specific light environment of the bench-top ePBR. Future studies regarding strain productivity, metabolic engineering, and stressors associated with mass cultivation in PBR should incorporate more realistic light environments into their experimental design. The fact that we observed such a drastic reduction in growth rate at higher densities in the ePBR suggests that there are major metabolic differences between cells grown in dynamic and rapidly changing light versus static light. We suggest that future investigations should begin incorporating additional stressors into experiments using realistic light environments. This will give insight into how dynamic changes in light intensities interact with other stressors to shape how photosynthesis and photoprotective mechanisms function.

MATERIALS AND METHODS

Culture Conditions and Growth Estimates

A Glc-tolerant strain of the model cyanobacterium *Synechocystis* sp. PCC 6803 (*Synechocystis* from here onward) gifted from the National Renewable Energy Laboratory (Dr. Jianping Yu) was grown axenically for the experiment described below. Cultures were maintained in BG-11 medium (Stanier et al., 1971) modified with 10 mM TES-NaOH buffer (pH 8), 2 mM Na_2CO_3, and an elevated

concentration of phosphate (0.106 M K_2HPO_4). All chemicals used were laboratory grade and purchased from either Thermo Fisher Scientific or Sigma-Aldrich.

Culture Conditions and Experimental Design

A 200-mL preculture was grown in 500-mL Erlenmeyer flasks in a Percival incubator at atmospheric CO_2, 30°C, and 12/12 h, 50 μmol photons m^{-2} s^{-1}/dark (Phillips F17T8/TL841/ALTO light tubes), on a rotating board at 100-rpm agitation for 1 week. The preculture was used to inoculate a custom-made glass vessel in an Environmental Photobioreactor v1 (ePBR; Phenometrics) to a final volume of 500 mL. The culture was sparged with 0.5 L min^{-1} 1% CO_2-enriched air and constantly stirred at 500 rpm. The surface light intensity was set to a 12-h sinusoidal function peaking at 2,000 μmol photons m^{-2} s^{-1} (Jallet et al., 2016a). For detailed information on the spectral properties of the LED, see Lucker et al. (2014), and for the custom-made glass vessel, see Supplemental Figure S2.

To approximate conditions of mass cultivation, we maintained the ePBR culture at a density corresponding to linear growth throughout the experiment. The culture was grown undiluted in batch mode for 4 d before being diluted to a density in midlinear growth phase at the end of the fourth day. After that, the culture was switched to semicontinuous growth mode through daily dilutions for at least 36 h prior to being sampled between the 7 and 10 incubation days. Depending on the type of sample collected, 5–13 sample points were taken, replacing an exact volume of 200 mL of the vessel each day. We chose this sampling scheme for two reasons: (1) it maintained the culture density and volume for a stable light environment within the ePBR, and (2) it allowed us to sample large volumes of culture (up to 10% of the total volume per sampling time) without depleting experimental replicates.

When describing diurnal time points of the ePBR, we use ZT based on circadian rhythm as described by van Alphen and Hellingwerf (2015). Throughout the paper, we refer to diurnal time points as ZT (i.e., hours past dawn), e.g., ZT1 corresponds to 1 h postdawn and ZT6, 6 h past dawn (or solar noon).

Culture Density, Cell Count, and Cell Size Measurements

Cell density was measured using a BD Accuri C6 Flow Cytometer (Agilent Technologies). At each time point, two technical 25-μL samples were diluted 1:40 in prefiltered (0.45 μm) BG-11. Pigment-containing cells, which constituted >95% of all recorded particles, were gated from nonviable particles using chl *a*/phycobilisome autofluorescence (640-nm excitation and 675 ± 25-nm emission detection). Because we used a semicontinuous cultivation method, we calculated doubling time based on an equation that accounted for the number of cells being extracted from the vessel, as well as any small net changes in cell density:

$$\text{doubling time (h)} = \frac{(C_{t1} - C_{t0}) + \sum (N_{\text{cells removed}})/V}{C_{\text{mean}}} \times (t_1 - t_0) \quad (1)$$

where C_{t1} is the cell density at the end time point, C_{t0} is the initial cell density, t_1 and t_0 are specific times of daily measurements (i.e., 24 h in between), $N_{\text{cells removed}}$ is the quantity of cells removed during sampling, V is the constant volume of the vessel (0.5 L), and C_{mean} is the average density of the culture between C_{t1} and C_{t0}, including measurements in between. It is important to note that this doubling time is specific to the density used in this experiment (OD_{750} of 0.73) since cells were growing linearly.

Cell volumes (referred to as biovolume from here on) were measured on 26 samples collected across 1 d from two experimental replicates. A 1-mL sample was centrifuged (5,000*g*, 5 min) and the pellet was resuspended in 100 μL of BG-11 and frozen at –20°C. Within 48 h, samples were thawed and imaged at 800× magnification using a Leica 5000 light microscope with a Hamamatsu C4742-95 digital camera. The area of >500 cells per sample was analyzed using ImageJ version 1.51 (National Institutes of Health; Abràmoff et al., 2004) and converted to biovolume assuming a spherical cell shape. The measured biovolume was used to calibrate the forward scatter measurement from flow cytometry (linear regression, $R^2 = 0.56$, $n = 26$), which was used to track changes in cell size across the experiment.

The in vivo absorption at 750 nm (OD_{750}) was monitored in a 1:10 diluted sample using a Cary 60 UV-Vis Spectrometer (Agilent Technologies). The OD_{750} was used as a proxy for culture density in the modeling of the cell-specific light environment.

CFD Modeling

As described in detail in Supplemental Data Set S1, CFD was used to simulate the movement of neutrally buoyant, 2-μm-diameter particles in the ePBR. The shape of the vessel (see Supplemental Fig. S2), speed of the rotation bar, sparging gas flow rate, and Reynolds number all affect the movement of the multiphase media and suspended particles. All governing equations and boundary conditions were modeled within the ANSYS Fluent framework. The model was validated using high-speed camera video recording of the movement of neutrally buoyant beads (1-mm diameter) in the ePBR vessel under the culture conditions described above. It was also validated against published results for similar systems (Perner-Nochta and Posten, 2007; Luo and Al-Dahhan, 2011). The cells move in and out of the light zones with a frequency of 0.17 s^{-1} in our ePBR, while the frequency is between 3 and 25 Hz in the bioreactor Perner-Nochta and Posten (2007) simulated with a helical mixer, indicating our ePBR represents a better mixing performance compared with their ePBR without active mixing. The predicted velocity magnitude is also in agreement when compared with the previous results of a draft tube airlift bioreactor simulated by Luo and Al-Dahhan (2011). The average velocity magnitude near the wall ranges from 0.15 to 0.30 m/s in our ePBR, which is close to their predicted values (0.4–0.6 m/s). Moreover, both sets of predictions show that the liquid has a larger velocity magnitude near the wall and has a smaller velocity magnitude near the center.

To accurately simulate the physics of both bubble and liquid motion, a multiphase volume of fluid model with a Euler-Euler approach was used to locate and track the free surface, whereby the two phases are treated as continua and it is assumed that the total volume fraction of each phase is constant (summing to unity) and continuous with respect to space and time (Hirt and Nichols, 1981). Conservation principles for mass and momentum are then applied to obtain pointwise governing equations for the simulation. The standard k-ε model was selected for this simulation, with a pressure-based solver to simulate the turbulence effect arising from the rotational motion of the stir bar and the introduced bubble column. This turbulence model includes two equations, one for turbulent kinetic energy (k) and the other for the specific dissipation rate (ε), which are used to enclose the Reynolds-averaged Navier-Stokes equations (Launder and Spalding, 1974). To predict the trajectories of individual *Synechocystis* cells in response to the bubble column and stir bar, the unsteady-state discrete phase model without particle-phase interaction was used. The shape of the cyanobacteria may be approximated as spherical, and thus a spherical drag law may be applied to calculate the drag force on any particle.

Particle motion was subsequently predicted using the computed three-dimensional flow field. A total of 6,204 particles were introduced into the liquid phase with uniform spacing, 27.0 s after flow was initiated by the stir bar and air addition; it was independently confirmed that the flow field is fully developed by this time by comparing the velocity contours against previous time steps and monitoring the location where the bubbles reach the interface. Once the individual cell trajectories were predicted, a supplemental MATLAB (MathWorks) code, developed for this study, was applied to perform statistical analysis on the data (Supplemental Data Sets S2 and S3). The frequency for the particles to reach the surface and bottom of the ePBR as well as the time intervals between these events were calculated with 1-ms resolution to analyze the pattern of the light environment experienced by the cyanobacteria over the course of a 24-h period. Additional details are provided in Supplemental Data Set S1.

Vertical Light Extinction in the ePBR

To understand the light environment within the ePBR, we conducted measurements on a culture at an OD_{750} between 0.62 and 0.85. We observed a degree of variability of PAR across the surface (1,000 ± 500 μmol photons m^{-2} s^{-1}) that depended on the distance from the center, but for the model we assumed that the surface light intensity was homogeneous. The PAR was measured at six discrete depths in the culture vessel at half-radius distance from the center (surface, 1-, 2-, 4-, 8-, and 23-cm depth) using a light meter (ULM-500; Walz) with a spherical detector. The light environment within the ePBR was modeled assuming a one-dimensional vertical extinction of light with culture depth. The average light intensity at a specific depth was used to calculate the absorption coefficient using Beer-Lambert law as described by Lee (1999):

$$A_x = \frac{\log_{10}(I_0/I_x)}{C\ D} \quad (2)$$

where I_x is the light intensity at depth x, I_0 is the light intensity at the surface, A_x is the calculated absorption coefficient at depth x, C is the density of the culture (in OD_{750}), and D is the depth in cm. Measurements were repeated at four different culture densities spanning the range of densities recorded during

the experiment (Supplemental Table S6). We observed that the absorption coefficient decreased with increasing depth (Supplemental Table S6), so Equation 2 was modified to include two absorption coefficients: one that governs the light extinction in the deep part of the reactor, and another close to the surface:

$$I_x = 10^{\left(\log_{10}[I_0(D/D_{max})] - A_{4cm}CD\right)} + 10^{\left(\log_{10}[I_0(1-D/D_{max})] - A_{23cm}CD\right)} \quad (3)$$

where A_{4cm} and A_{23cm} are the absorption coefficients calculated based on the light intensity measured at 4- and 23-cm depth, respectively, and D_{max} is the depth at the bottom of the vessel (23 cm).

Synthesized Model of the Cell-Specific Light Environment of the ePBR

The methods described in the previous section allowed us to model both the diurnal and rapid (microsecond resolution) fluctuation in incident light that an individual cell is subjected to as it mixes through the ePBR. This was accomplished by synthesizing the vertical light extinction model (Eq. 3) with the sinusoidal change in surface light intensity given by Jallet et al. (2016a) and the vertical tracking of a single cell over the course of 24 h, using the CFD model described in the previous section. This generated a high-resolution model of the light intensity experienced by a single cell over the course of a day, which is referred to hence forth as the cell-specific light environment.

Chl *a* and Total Carotenoid Quantification

The absorption spectra of pigments in methanol was recorded using a Cary 60 UV-Vis spectrometer (Agilent Technologies). 0.01% (v/v) Tween 20 was added to a 1.5-mL sample, which was centrifuged at 5,000*g* for 5 min; the resulting pellet was dissolved in methanol; and pigments were extracted overnight at –20°C. Chl *a* concentrations in the extract were calculated according to previous methodology (Ritchie, 2006), and the total carotenoid content was deconvoluted from chl *a* using previously published equations (Wellburn, 1994). The ratio of total carotenoids to chl *a* was calculated on a w/w basis.

TOC and Nitrogen Content

To estimate rates of carbon accumulation in the culture, TOC and nitrogen were analyzed using a Shimadzu TOC-L Laboratory TOC Analyzer. We used the method described by Caballero et al. (2016), with modifications to the cell-harvesting protocol as described below. A 1.5-mL culture sample was centrifuged in acid-washed (10% [v/v] HCl) Eppendorf tubes at 5,000*g* for 5 min. The pellet was washed in 1 mL of ice cold 0.041 N NaCl solution (isotonic to BG-11) with 0.01% (v/v) Tween 20, and the cell density of the washed cells was measured using flow cytometry. Cells were centrifuged a second time (5,000*g*, 5 min), the supernatant was removed, and the pellet was immediately frozen and stored at –80°C.

Pulse Amplitude–Modulated Chl *a* Fluorescence, Net-Oxygen Evolution, and Rapid Oxygen Versus Irradiance Curves

The photosynthetic capacity of *Synechocystis* was assayed using a combination of chl *a*/phycobilisome fluorescence and oxygen evolution measurements. A Walz DUAL-PAM 100 fluorometer equipped with a custom-made, aluminum cuvette holder and a FireSting OXROB10 probe connected to a Optical Oxygen Meter (FireSting) was used to detect chl *a*/phycobilisome fluorescence and changes in oxygen concentration mirroring net-oxygen evolution and dark consumption rates. The oxygen probe was calibrated against air-saturated and anoxic BG-11, which was instigated through the addition of sodium sulfite, which rapidly reacts with and consumes molecular oxygen. We utilized the ePBR's white LED light as an actinic light source to more closely approximate conditions of the ePBR. In tandem, the measuring light (620 nm) and saturating pulses (300 ms, 10,000 μmol photons m^{-2} s^{-1}, 654 nm) of the DUAL-PAM were used to monitor F_0' and elicit F_M'. F_0 corresponds to the fluorescence of cells in darkness, whereas F_M is measured during the saturating flash. The aluminum cuvette holder was maintained at 30°C through internal circulation of heated water from an Isotemp water bath (Thermo Fisher Scientific).

Rapid light curves were generated using a range of relevant light intensities (2.5, 15, 21, 47, 56, 92, 119, 125, 165, 356, 600, 950, 1,200, 1,400 μmol photons m^{-2} s^{-1}) using 1-min intervals (MacIntyre et al., 2002). Fifty-microliter samples were pulled from the ePBR at specific time points and preincubated under low white light (20 μmol photons m^{-2} s^{-1}) in a 250-mL Erlenmeyer flask for 10 min to relax NPQ and other rapidly reversible photoprotective mechanisms. Measurements were taken on a 1.5-mL subsample enriched with 10 mM sodium bicarbonate in a cylindrical quartz cuvette. Dark respiration rates and estimations of F_0 were measured during an initial 5-min dark treatment, after which the actinic light intensities were applied in an incremental fashion.

Light response parameters were calculated as previously described (Eilers and Peeters, 1988; Jallet et al., 2016a), where P_{max} corresponds to the maximum rate of photosynthesis, E_k is the irradiance saturation index, and α is the linear coefficient of the light-limited slope. For the purposes of defining the optimal irradiance for photosynthesis ($E_{optimum}$) and the half-point saturation of photosynthesis ($P_{max\text{-}half}$), we used the wait-in-line model using the Excel (Microsoft) calculations provided by Ritchie (2008).

NPQ versus Irradiance

The fluorescence trace collected during the P-I curves was used to quantify the level of NPQ at specific irradiances. Each light step was ended with a saturating pulse, and the nonsteady-state NPQ was estimated as the relative quenching of F_M through the equation $1 - F_M'/F_M$ (Wilson et al., 2006). We chose not to use traditional NPQ calculations, such as the Stern-Volmer equation, since cyanobacteria have a different quenching mechanism than plants and most algae (Kirilovsky, 2007). A representative example of fluorescence trace is shown in Supplemental Figure S6.

Chlorophyll Fluorometry of In Situ Physiology

The F_V/F_M was measured as an indicator of photoinhibition or modifications to the redox state of the plastoquinone pool. Within 30 s of removing a sampling from the ePBR, F_V/F_M was measured using a FIRe Fluorometer (Satlantic; Kolber et al., 1998). This system utilizes a blue excitation light (excitation at 450 nm, emission measured at 678 nm), which dampens the interference of the *Synechocystis* phycobilisome fluorescence by targeting the soret band unique to the chl *a* absorption spectra (Elmorjani et al., 1986; Vernotte et al., 1992). F_0 corresponds to the fluorescence of cells in darkness, and a 400-ms single-turnover flash (27,500 μmol photons m^{-2} s^{-1}, 475 nm) was used to elicit F_M.

We used a Walz DUAL-PAM 100 fluorometer with a red measuring light (620 nm) to estimate quenching of chl *a*/phycobilisome fluorescence and distinguish between OCP-quenching and state transition. The maximum variable fluorescence due to state transition was based on the low blue light (26 μmol photons m^{-2} s^{-1} at 430 nm) acclimatized state (state I; high fluorescence) versus the dark acclimatized state (state II; low fluorescence). An example of a fluorescence trace is shown in Supplemental Figure S6B, with the equation for state transition quenching ($1 - F_{Md}/F_M$) describing the capacity for state transition (Mullineaux and Emlyn-Jones, 2005).

OCP-dependent quenching of fluorescence is a high light–induced photoprotective mechanism, and it was elicited as described by Wilson et al. (2006) and measured with the red measuring light (620 nm) of the DUAL-PAM, with modifications described below. The in situ level of quenched fluorescence (F_{M60}) was based on the measured F_M' 60 s after the sample was extracted from the ePBR, including a treatment with 10 s of low blue actinic light treatment (26 μmol photons m^{-2} s^{-1} of 430 nm) to promote state I transition. F_M was based on the maximum recovery of F_M' under continued low blue actinic light treatment. Thus, the level of in situ OCP-dependent quenching ($OCP_{in\ situ}$-quenching) was estimated as $OCP_{in\ situ}$-quenching $= (1 - F_{M60}/F_M)$ according to the fluorescence trace shown in Supplemental Figure S6C. The maximum capacity for fluorescence quenching was measured by applying a strong blue actinic light (880 μmol photons m^{-2} s^{-1}) for 7 min and recording the maximum quenching of F_M' (F_{Mg}^*). The maximal capacity for fluorescence quenching was calculated as OCP_{max} quenching $= (F_{Mg}^*/F_M)$. In this study, we consider fluorescence parameters based on measurements taken within 1 min of removing the sample from the ePBR to represent in situ conditions, which was validated by the relatively slow relaxation kinetics of OCP_{max} quenching (Supplemental Fig. S6C).

Quantification of Oxygen Production and Consumption Ex Situ Using MIMS

We designed an experiment to investigate the physiological response of *Synechocystis* to the predicted cell-specific light environment of the ePBR.

By applying a fluctuating light treatment ex situ, we could synchronize a population of cells to the unique cell-specific conditions of the ePBR, as predicted by our cell-specific light model. We used the actinic lights of the DUAL-PAM to recreate the light environment of a single cell using one-part blue (430 nm) to two-parts red (635 nm). We selected a representative 5-min section of the CFD model (see Supplemental Fig. S7 and Supplemental Data Set S4) and modified the surface light intensity according to the time of day (see Supplemental Table S3). The 620-nm measuring light of the DUAL-PAM was used.

We used MIMS to partition between illuminated rates of oxygen production and consumption (Allahverdiyeva et al., 2013; Ermakova et al., 2016). In brief, a QMS-100 (Pfeiffer Vacuum) fitted with a 0.2-μm-thick silicon membrane was used to measure oxygen production ($^{16}O_2$ derived from H_2O) and consumption ($^{16}O_2$ and $^{18}O_2$ reduced to water). The design of the MIMS and DUAL-PAM set-up can be seen in Supplemental Figure S11. A 25-mL culture sample was centrifuged (3,220*g*, 10 min), and the cell pellet was resuspended in BG-11 plus 10 mM HCO_3 to a chl *a* concentration of 15 μg mL^{-1}. Two milliliters of the culture was incubated in the MIMS and the dissolved oxygen concentration was reduced to approximately 25% of atmospheric saturation through equilibration with 100% N_2 gas. The removed oxygen was replaced with pure isotopic $^{18}O_2$.

The isotopic enrichment process was conducted under dim light (>5 μmol photons m^{-2} s^{-1}) and lasted ~10 min. After that, dark respiration was measured for 5 min followed by a 3-min static light treatment and four loops of the 5-min fluctuating light treatment (see Supplemental Data Set S4). Due to the small volume of the cuvette and the continuous consumption of gases by the MIMS, there was a significant net extraction of dissolved gases (approximately 30% per hour). To account for abiotic consumption of gases and changes in partial pressure, we normalized the oxygen traces to argon ($m/z = 40$). Oxygen evolution (gross photosynthesis) and consumption (respiration and AET) during the different treatments were calculated as previously described by Bailleul et al. (2017).

Statistical Analysis

All data used for the statistical analysis were gathered from independent experimental replicates and analyzed using Sigma Plot (v 1.3; Systat Software). RM-ANOVAs, with time as a fixed variable, were used to analyze diurnal changes in physiological variables of the ePBR cultures. One-way ANOVA was used to compare response variables between different growth conditions. If significant, temporal and treatment differences were further analyzed using Tukey's post hoc test. Samples with $P < 0.05$ were considered statistically different, and data are shown as averages ± 1 SD (SD) throughout the text. F-statistics are presented with the degrees of freedom between groups (time points or treatments) followed by the total degrees of freedom (between measuring points) as $F_{\text{df(time-points, df(measuring-points)}}$.

Supplemental Data

The following supplemental materials are available.

Supplemental Figure S1. Comparison of growth rates in the ePBR versus Erlenmeyer flasks commonly used in laboratory experiments.

Supplemental Figure S2. Geometrical model of the ePBR vessel accompanied by real images.

Supplemental Figure S3. Detailed illustration of the velocity profiles of the four cross sections shown in Figure 3.

Supplemental Figure S4. Frequency and length of events when a particle (cell) enters the surface and bottom zones.

Supplemental Figure S5. The spectrum of the ePBR LED light (surface) and changes as the light penetrates deeper into the culture (2, 4, and 8 cm depth).

Supplemental Figure S6. Fluorescence traces used to quantify NPQ.

Supplemental Figure S7. Selection of the ex situ fluctuating light treatment.

Supplemental Figure S8. Illuminated rates of oxygen evolution and consumption during the ex situ fluctuating light experiment.

Supplemental Figure S9. The incident light regime used to test fluctuating light versus constant light on growth of dilute *Synechocystis* cultures in the ePBR.

Supplemental Figure S10. Spectral composition of actinic light used in the ex situ fluctuating light experiments.

Supplemental Figure S11. Set-up of the MIMS with the Dual Pulse PAM fluorometer.

Supplemental Table S1. Diurnal changes in physiological parameters of *Synechocystis* growing in the ePBR.

Supplemental Table S2. Comparison between physiological parameters of cultures grown in the ePBR and Erlenmeyer flask under continuous low light (30 μmol photons m^{-2} s^{-1}) and high light (400 μmol photons m^{-2} s^{-1}).

Supplemental Table S3. Surface/maximum and time-integrated PAR used at specific times of the ex situ fluctuating light experiment.

Supplemental Table S4. Parameters derivate form the rapid photosynthesis versus irradiance curves.

Supplemental Table S5. Photosynthesis versus irradiance parameters contrasting the PAM's actinic light with the ePBR's white LED light.

Supplemental Table S6. Measured light intensities (PAR) at specific depths of the ePBR and with different culture densities.

Supplemental Data Set S1. Description of CFD model.

Supplemental Data Set S2. User-defined function written in C and linked to the ANSYS Fluent simulations to prevent spurious particle passage from the liquid into the air at the upper interface.

Supplemental Data Set S3. MATLAB scripts used to visualize the trajectories of the particles and plot the instantaneous location of the particles.

Supplemental Data Set S4. Excel sheet showing changes in light used to test the effects of fluctuating light on photophysiology ex situ.

Supplemental Video. Illustration of the computational fluid dynamic simulation of the ePBR with temporal resolution.

ACKNOWLEDGMENTS

The authors thank Denis Jallet, Michael Caballero, Alexander Hughes, and David Xing for experimental assistance, advice, and critical reviewing during the preparation of the manuscript. Gus Waneka helped develop the ImageJ protocol for measuring cell sizes. Mark Layer wrote the fluctuating light scripts.

Received April 24, 2019; accepted July 15, 2019; published August 7, 2019.

LITERATURE CITED

Abràmoff MD, Magalhães PJ, Ram SJ (2004) Image processing with ImageJ. Biophoton Int **11:** 36–42

Acuña AM, Kaňa R, Gwizdala M, Snellenburg JJ, van Alphen P, van Oort B, Kirilovsky D, van Grondelle R, van Stokkum IHM (2016) A method to decompose spectral changes in *Synechocystis* PCC 6803 during light-induced state transitions. Photosynth Res **130:** 237–249

Allahverdiyeva Y, Mustila H, Ermakova M, Bersanini L, Richaud P, Ajlani G, Battchikova N, Cournac L, Aro E-M (2013) Flavodiiron proteins Flv1 and Flv3 enable cyanobacterial growth and photosynthesis under fluctuating light. Proc Natl Acad Sci USA **110:** 4111–4116

Angermayr SA, Gorchs Rovira A, Hellingwerf KJ (2015) Metabolic engineering of cyanobacteria for the synthesis of commodity products. Trends Biotechnol **33:** 352–361

Bailleul B, Park J, Brown CM, Bidle KD, Lee SH, Falkowski PG (2017) Direct measurements of the light dependence of gross photosynthesis and oxygen consumption in the ocean. Limnol Oceanogr **62:** 1066–1079.

Barbosa MJ, Janssen M, Ham N, Tramper J, Wijffels RH (2003) Microalgae cultivation in air-lift reactors: Modeling biomass yield and growth rate as a function of mixing frequency. Biotechnol Bioeng **82:** 170–179

Behrenfeld MJ, Kolber ZS (1999) Widespread iron limitation of phytoplankton in the South Pacific Ocean. Science **283:** 840–843

Behrenfeld MJ, Prasil O, Babin M, Bruyant F (2004) In search of a physiological basis for covariations in light-limited and light-saturated photosynthesis. J Phycol **40:** 4–25

Bersanini L, Battchikova N, Jokel M, Rehman A, Vass I, Allahverdiyeva Y, Aro E-M (2014) Flavodiiron protein Flv2/Flv4-related photoprotective mechanism dissipates excitation pressure of PSII in cooperation with phycobilisomes in cyanobacteria. Plant Physiol **164:** 805–818

Bersanini L, Allahverdiyeva Y, Battchikova N, Heinz S, Lespinasse M, Ruohisto E, Mustila H, Nickelsen J, Vass I, Aro E-M (2017) Dissecting the photoprotective mechanism encoded by the flv4-2 operon: A distinct contribution of Sll0218 in photosystem II stabilization. Plant Cell Environ **40:** 378–389

Berteotti S, Ballottari M, Bassi R (2016) Increased biomass productivity in green algae by tuning non-photochemical quenching. Sci Rep **6:** 21339

Bitog JP, Lee IB, Lee CG, Kim KS, Hwang HS, Hong SW, Seo IH, Kwon KS, Mostafa E (2011) Application of computational fluid dynamics for modeling and designing photobioreactors for microalgae production: A review. Comput Electron Agric **76:** 131–147

Brennan L, Owende P (2010) Biofuels from microalgae—A review of technologies for production, processing, and extractions of biofuels and co-products. Renew Sustain Energy Rev **14:** 557–577

Caballero MA, Jallet D, Shi L, Rithner C, Zhang Y, Peers G (2016) Quantification of chrysolaminarin from the model diatom *Phaeodactylum tricornutum*. Algal Res **20:** 180–188

Calvo F, Bula A, Di Mare L, Garcia S (2017) CFD simulation of multiphase (liquid-solid-gas) flow in an airlift column photobioreactor. Acta Mech **228:** 2413–2427

Derks A, Schaven K, Bruce D (2015) Diverse mechanisms for photoprotection in photosynthesis. Dynamic regulation of photosystem II excitation in response to rapid environmental change. Biochim Biophys Acta **1847:** 468–485

Devarapalli M, Lawrence BJ, Madihally SV (2009) Modeling nutrient consumptions in large flow-through bioreactors for tissue engineering. Biotechnol Bioeng **103:** 1003–1015

Dhanasekharan KM, Sanyal J, Jain A, Haidari A (2005) A generalized approach to model oxygen transfer in bioreactors using population balances and computational fluid dynamics. Chem Eng Sci **60:** 213–218

Dimier C, Brunet C, Geider R, Raven J (2009) Growth and photoregulation dynamics of the picoeukaryote *Pelagomonas calceolata* in fluctuating light. Limnol Oceanogr **54:** 823–836

Du W, Jongbloets JA, Hernández HP, Bruggeman FJ, Hellingwerf KJ, dos Santos FB (2016) Photonfluxostat: A method for light-limited batch cultivation of cyanobacteria at different, yet constant, growth rates. Algal Res **20:** 118–125

Eilers P, Peeters J (1988) A model for the relationship between light intensity and the rate of photosynthesis in phytoplankton. Ecol Modell **42:** 199–215

Elmorjani K, Thomas J-C, Sebban P (1986) Phycobilisomes of wild type and pigment mutants of the cyanobacterium *Synechocystis* PCC 6803. Arch Microbiol **146:** 186–191

Emlyn-Jones D, Ashby MK, Mullineaux CW (1999) A gene required for the regulation of photosynthetic light harvesting in the cyanobacterium *Synechocystis* 6803. Mol Microbiol **33:** 1050–1058

Erickson E, Wakao S, Niyogi KK (2015) Light stress and photoprotection in *Chlamydomonas reinhardtii*. Plant J **82:** 449–465

Ermakova M, Huokko T, Richaud P, Bersanini L, Howe CJ, Lea-Smith DJ, Peltier G, Allahverdiyeva Y (2016) Distinguishing the roles of thylakoid respiratory terminal oxidases in the cyanobacterium *Synechocystis* sp. PCC 6803. Plant Physiol **171:** 1307–1319

Esteves-Ferreira AA, Inaba M, Obata T, Fort A, Fleming GTA, Araújo WL, Fernie AR, Sulpice R (2017) A novel mechanism, linked to cell density, largely controls cell division in *Synechocystis*. Plant Physiol **174:** 2166–2182

Gao X, Kong B, Vigil RD (2017) Comprehensive computational model for combining fluid hydrodynamics, light transport and biomass growth in a Taylor vortex algal photobioreactor: Eulerian approach. Algal Res **24:** 1–8

Hihara Y, Kamei A, Kanehisa M, Kaplan A, Ikeuchi M (2001) DNA microarray analysis of cyanobacterial gene expression during acclimation to high light. Plant Cell **13:** 793–806

Hihara Y, Sonoike K, Kanehisa M, Ikeuchi M (2003) DNA microarray analysis of redox-responsive genes in the genome of the cyanobacterium *Synechocystis* sp. strain PCC 6803. J Bacteriol **185:** 1719–1725

Hirt CW, Nichols BD (1981) Volume of fluid (VOF) method for the dynamics of free boundaries. J Comput Phys **39:** 201–225

Huang J, Li Y, Wan M, Yan Y, Feng F, Qu X, Wang J, Shen G, Li W, Fan J, et al (2014) Novel flat-plate photobioreactors for microalgae cultivation with special mixers to promote mixing along the light gradient. Bioresour Technol **159:** 8–16

Huang J, Feng F, Wan M, Ying J, Li Y, Qu X, Pan R, Shen G, Li W (2015) Improving performance of flat-plate photobioreactors by installation of novel internal mixers optimized with computational fluid dynamics. Bioresour Technol **182:** 151–159

Huang J, Ying J, Fan F, Yang Q, Wang J, Li Y (2016) Development of a novel multi-column airlift photobioreactor with easy scalability by means of computational fluid dynamics simulations and experiments. Bioresour Technol **222:** 399–407

Hutmacher DW, Singh H (2008) Computational fluid dynamics for improved bioreactor design and 3D culture. Trends Biotechnol **26:** 166–172

Jallet D, Caballero MA, Gallina AA, Youngblood M, Peers G (2016a) Photosynthetic physiology and biomass partitioning in the model diatom *Phaeodactylum tricornutum* grown in a sinusoidal light regime. Algal Res **18:** 51–60

Jallet D, Cantrell M, Peers G (2016b) New players for photoprotection and light acclimation. *In* H Kirchhoff, ed, Chloroplasts: Current Research and Future Trends. Caister Academic Press, Norfolk, United Kingdom, pp 135–160

Jameson A (1995) Optimum aerodynamic design using control theory. Computational Fluid Dynamics Review **3:** 495–528

Kaiser E, Morales A, Harbinson J (2018) Fluctuating light takes crop photosynthesis on a rollercoaster ride. Plant Physiol **176:** 977–989

Kaneko T, Sato S, Kotani H, Tanaka A, Asamizu E, Nakamura Y, Miyajima N, Hirosawa M, Sugiura M, Sasamoto S, et al (1996) Sequence analysis of the genome of the unicellular cyanobacterium *Synechocystis* sp. strain PCC6803. II. Sequence determination of the entire genome and assignment of potential protein-coding regions. DNA Res **3:** 109–136

Kayahan E, Eroglu I, Koku H (2016) Design of an outdoor stacked-tubular reactor for biological hydrogen production. Int J Hydrogen Energy **41:** 19357–19366

Kim HW, Vannela R, Zhou C, Rittmann BE (2011) Nutrient acquisition and limitation for the photoautotrophic growth of *Synechocystis* sp. PCC6803 as a renewable biomass source. Biotechnol Bioeng **108:** 277–285

Kirilovsky D (2007) Photoprotection in cyanobacteria: The orange carotenoid protein (OCP)-related non-photochemical-quenching mechanism. Photosynth Res **93:** 7–16

Kirilovsky D (2015) Modulating energy arriving at photochemical reaction centers: Orange carotenoid protein-related photoprotection and state transitions. Photosynth Res **126:** 3–17

Kirst H, Formighieri C, Melis A (2014) Maximizing photosynthetic efficiency and culture productivity in cyanobacteria upon minimizing the phycobilisome light-harvesting antenna size. Biochim Biophys Acta **1837:** 1653–1664

Koksharova OA, Wolk CP (2002) Genetic tools for cyanobacteria. Appl Microbiol Biotechnol **58:** 123–137

Kolber ZS, Prášil O, Falkowski PG (1998) Measurements of variable chlorophyll fluorescence using fast repetition rate techniques: Defining methodology and experimental protocols. Biochim Biophys Acta **1367:** 88–106

Kramer DM, Evans JR (2011) The importance of energy balance in improving photosynthetic productivity. Plant Physiol **155:** 70–78

Kromdijk J, Głowacka K, Leonelli L, Gabilly ST, Iwai M, Niyogi KK, Long SP (2016) Improving photosynthesis and crop productivity by accelerating recovery from photoprotection. Science **354:** 857–861

Launder BE, Spalding DB (1974) The numerical computation of turbulent flows. Comput Methods Appl Mech Eng **3:** 269–289

Lea-Smith DJ, Ross N, Zori M, Bendall DS, Dennis JS, Scott SA, Smith AG, Howe CJ (2013) Thylakoid terminal oxidases are essential for the cyanobacterium *Synechocystis* sp. PCC 6803 to survive rapidly changing light intensities. Plant Physiol **162:** 484–495

Lee C-G (1999) Calculation of light penetration depth in photobioreactors. Biotechnol Bioprocess Eng; BBE **4:** 78–81

Liffman K, Paterson DA, Liovic P, Bandopadhayay P (2013) Comparing the energy efficiency of different high rate algal raceway pond designs using computational fluid dynamics. Chem Eng Res Des **91:** 221–226

Liu S-W, Qiu B-S (2012) Different responses of photosynthesis and flow cytometric signals to iron limitation and nitrogen source in coastal and oceanic *Synechococcus* strains (Cyanophyceae). Mar Biol **159:** 519–532

Lucker BF, Hall CC, Zegarac R, Kramer DM (2014) The environmental photobioreactor (ePBR): An algal culturing platform for simulating dynamic natural environments. Algal Res **6:** 242–249

Luo H-P, Al-Dahhan MH (2011) Verification and validation of CFD simulations for local flow dynamics in a draft tube airlift bioreactor. Chem Eng Sci **66:** 907–923

MacIntyre HL, Kana TM, Anning T, Geider RJ (2002) Photoacclimation of photosynthesis irradiance response curves and photosynthetic pigments in microalgae and cyanobacteria. J Phycol **38:** 17–38

Masojidek J, Papacek S, Sergejevova M, Jirka V, Cerveny J, Kunc J, Korecko J, Verbovikova O, Kopecky J, Stys D, et al (2003) A closed solar photobioreactor for cultivation of microalgae under supra-high irradiance: basic design and performance. J Appl Phycol **15:** 239–248

McClung CR (2006) Plant circadian rhythms. Plant Cell **18:** 792–803

Melis A (2009) Solar energy conversion efficiencies in photosynthesis: Minimizing the chlorophyll antennae to maximize efficiency. Plant Sci **177:** 272–280

Mullineaux CW, Allen JF (1990) State 1-State 2 transitions in the cyanobacterium *Synechococcus* 6301 are controlled by the redox state of electron carriers between photosystems I and II. Photosynth Res **23:** 297–311

Mullineaux CW, Emlyn-Jones D (2005) State transitions: An example of acclimation to low-light stress. J Exp Bot **56:** 389–393

Nedbal L, Tichy V, Xiong FH, Grobbelaar JU (1996) Microscopic green algae and cyanobacteria in high-frequency intermittent light. J Appl Phycol **8:** 325–333

Ort DR, Merchant SS, Alric J, Barkan A, Blankenship RE, Bock R, Croce R, Hanson MR, Hibberd JM, Long SP, et al (2015) Redesigning photosynthesis to sustainably meet global food and bioenergy demand. Proc Natl Acad Sci USA **112:** 8529–8536

Oxborough K, Horton P (1988) A study of the regulation and function of energy-dependent quenching in pea chloroplasts. Biochimica Biophysica Acta Bioenergetics **934:** 135–143

Park S, Li Y (2015) Integration of biological kinetics and computational fluid dynamics to model the growth of *Nannochloropsis salina* in an open channel raceway. Biotechnol Bioeng **112:** 923–933

Peers G (2014) Increasing algal photosynthetic productivity by integrating ecophysiology with systems biology. Trends Biotechnol **32:** 551–555

Peers G (2015) Enhancement of biomass production by disruption of light energy dissipation pathways. United States of America Patent Application No. 8,940,508.

Perner-Nochta I, Posten C (2007) Simulations of light intensity variation in photobioreactors. J Biotechnol **131:** 276–285

Posten C (2009) Design principles of photo-bioreactors for cultivation of microalgae. Eng Life Sci **9:** 165–177

Prussi M, Buffi M, Casini D, Chiaramonti D, Martelli F, Carnevale M, Tredici MR, Rodolfi L (2014) Experimental and numerical investigations of mixing in raceway ponds for algae cultivation. Biomass Bioenergy **67:** 390–400

Retkute R, Townsend AJ, Murchie EH, Jensen OE, Preston SP (2018) Three-dimensional plant architecture and sunlit-shaded patterns: A stochastic model of light dynamics in canopies. Ann Bot **122:** 291–302

Ritchie RJ (2006) Consistent sets of spectrophotometric chlorophyll equations for acetone, methanol and ethanol solvents. Photosynth Res **89:** 27–41

Ritchie RJ (2008) Fitting light saturation curves measured using modulated fluorometry. Photosynth Res **96:** 201–215

Ritchie RJ, Larkum AWD (2012) Modelling photosynthesis in shallow algal production ponds. Photosynthetica **50:** 481–500

Schuurmans RM, van Alphen P, Schuurmans JM, Matthijs HCP, Hellingwerf KJ (2015) Comparison of the photosynthetic yield of cyanobacteria and green algae: Different methods give different answers. PLoS One **10:** e0139061

Shimakawa G, Shaku K, Nishi A, Hayashi R, Yamamoto H, Sakamoto K, Makino A, Miyake C (2015) FLAVODIIRON2 and FLAVODIIRON4 proteins mediate an oxygen-dependent alternative electron flow in *Synechocystis* sp. PCC 6803 under CO2-limited conditions. Plant Physiol **167:** 472–480

Simionato D, Basso S, Giacometti GM, Morosinotto T (2013) Optimization of light use efficiency for biofuel production in algae. Biophys Chem **182:** 71–78

Soman A, Shastri Y (2015) Optimization of novel photobioreactor design using computational fluid dynamics. Appl Energy **140:** 246–255

Stanier RY, Kunisawa R, Mandel M, Cohen-Bazire G (1971) Purification and properties of unicellular blue-green algae (order Chroococcales). Bacteriol Rev **35:** 171–205

Takache H, Pruvost J, Marec H (2015) Investigation of light/dark cycles effects on the photosynthetic growth of *Chlamydomonas reinhardtii* in conditions representative of photobioreactor cultivation. Algal Res **8:** 192–204

Townsend AJ, Retkute R, Chinnathambi K, Randall JWP, Foulkes J, Carmo-Silva E, Murchie EH (2018) Suboptimal acclimation of photosynthesis to light in wheat canopies. Plant Physiol **176:** 1233–1246

van Alphen P, Hellingwerf KJ (2015) Sustained circadian rhythms in continuous light in *Synechocystis* sp. PCC6803 growing in a well-controlled photobioreactor. PLoS One **10:** e0127715

Vernotte C, Picaud M, Kirilovsky D, Olive J, Ajlani G, Astier C (1992) Changes in the photosynthetic apparatus in the cyanobacterium *Synechocystis* sp. PCC 6714 following light-to-dark and dark-to-light transitions. Photosynth Res **32:** 45–57

Vialet-Chabrand S, Matthews JSA, Simkin AJ, Raines CA, Lawson T (2017) Importance of fluctuations in light on plant photosynthetic acclimation. Plant Physiol **173:** 2163–2179

Wellburn AR (1994) The spectral determination of chlorophylls a and b, as well as total carotenoids, using various solvents with spectrophotometers of different resolution. J Plant Physiol **144:** 307–313

Wilson A, Ajlani G, Verbavatz JM, Vass I, Kerfeld CA, Kirilovsky D (2006) A soluble carotenoid protein involved in phycobilisome-related energy dissipation in cyanobacteria. Plant Cell **18:** 992–1007

Yarnold J, Ross IL, Hankamer B (2016) Photoacclimation and productivity of *Chlamydomonas reinhardtii* grown in fluctuating light regimes which simulate outdoor algal culture conditions. Algal Res **13:** 182–194

Zhang P, Eisenhut M, Brandt AM, Carmel D, Silén HM, Vass I, Allahverdiyeva Y, Salminen TA, Aro EM (2012) Operon flv4-flv2 provides cyanobacterial photosystem II with flexibility of electron transfer. Plant Cell **24:** 1952–1971

Zhu X-G, Long SP, Ort DR (2010) Improving photosynthetic efficiency for greater yield. Annu Rev Plant Biol **61:** 235–261